Research Square

Preprints are preliminary reports that have not undergone peer review.
They should not be considered conclusive, used to inform clinical practice,
or referenced by the media as validated information.

Transduction of inflammation from peripheral immune cells to the hippocampus induces neuronal hyperexcitability mediated by Caspase-1 activation

Tarek Shaker (tarek.shaker@umontreal.ca)
Universite de Montreal - Centre de recherche du CHU Sainte Justine https://orcid.org/0000-0001-8329-4101

Bidisha Chattopadhyaya
Centre Hospitalier Universitaire Sainte-Justine

Bénédicte Amilhon
Universite de Montreal

Graziella Di Cristo
Universite de Montreal

Alexander G. Weil
Universite de Montreal

Research

Keywords: Caspase-1, hippocampus, hyperexcitability, inflammasome, organotypic cultures, peripheral blood mononuclear cells

Posted Date: March 25th, 2020

DOI: https://doi.org/10.21203/rs.3.rs-19156/v1

License: This work is licensed under a Creative Commons Attribution 4.0 International License.
Read Full License

Version of Record: A version of this preprint was published at Neurobiology of Disease on December 1st, 2021. See the published version at https://doi.org/10.1016/j.nbd.2021.105535.

Abstract

Background

Recent studies report infiltration of peripheral blood mononuclear cells (PBMCs) into the central nervous system (CNS) in epileptic disorders, suggestive of a potential contribution of PBMC extravasation to the generation of seizures. Nevertheless, the underlying mechanisms involved in PBMC infiltrates promoting neuronal predisposition to ictogenesis remain unclear. Therefore, we developed an in vitro model mimicking PBMC infiltration into the brain in order to investigate potential transduction of inflammatory signals from PBMCs to the CNS.

Methods

To establish our model, we first extracted PBMCs from rat spleen, then, we immunologically primed PBMCs with lipopolysaccharide (LPS), followed by immunological activation with Nigericin. Thereafter, we cultured PBMCs on top of organotypic cortico-hippocampal brain slice cultures (OCHSCs) derived from the same rat, and compared PBMC-OCHSC co-cultures to OCHSCs exposed to PBMCs in the culture media. Also, we targeted a potential molecular pathway underlying transduction of peripheral inflammation to OCHSCs by incubating OCHSCs with the Caspase-1 inhibitor VX-765 prior to co-culturing PBMCs with OCHSCs. After 24 hours, we immunohistochemically analyzed inflammation markers in the cortex and the hippocampus. In addition, we performed whole-cell patch-clamp recordings in cortical layer II/III and hippocampal CA1 pyramidal neurons.

Results

In the cortex, co-culturing immunoreactive PBMCs treated with LPS + Nigericin on top of OCHSCs induced ectopic expression of inflammation markers and enhanced neuronal excitation. In contrast, no excitability changes were detected after adding primed PBMCs, i.e. treated with LPS only, to OCHSCs. Strikingly, in the hippocampus, both immunoreactive and primed PBMCs elicited similar pro-inflammatory and pro-excitatory effects. However, when immunoreactive and primed PBMCs were cultured in the media separately from OCHSCs, only immunoreactive PBMCs gave rise to neuroinflammation and hyperexcitability in the hippocampus, whereas primed PBMCs failed to produce any significant changes. Finally, VX-765 application to OCHSCs, co-cultured with either immunoreactive or primed PBMCs, protected them from neuroinflammation and hippocampal hyperexcitability.

Conclusions

Our study shows a higher susceptibility of the hippocampus to peripheral inflammation as compared to the cortex, mediated via Caspase-1-dependent signaling pathways. Thus, our findings suggest that Caspase-1 inhibition may potentially provide therapeutic benefits during hippocampal neuroinflammation and hyperexcitability secondary to peripheral innate immunity.

Introduction

Systemic inflammation following pathogenic and non-pathogenic sterile insults has been linked to the subsequent development of epileptic disorders, such as febrile infection-related epilepsy syndrome (1), temporal lobe epilepsy associated with prolonged febrile seizures (2) and Rasmussen encephalitis (3). Nevertheless, it is yet to be determined how systemic inflammation contributes to the pathogenesis of epileptic seizures. Recent evidence suggests that penetration of peripheral immune cells, namely peripheral blood mononuclear cells (PBMCs), into the central nervous system (CNS) following peripheral inflammation may potentially render the brain vulnerable to epileptogenesis. Indeed, experimental epilepsy models indicate that the presence of PBMC infiltrates in the brain promotes seizure development (4, 5). Yet, evoking peripheral inflammation in experimental animals revealed that cellular and molecular mechanisms beside PBMCs recruitment to the brain also play key roles in inflammation-induced facilitation of epileptiform activity. Such inflammatory processes include pro-inflammatory cytokines infiltrating the blood-brain barrier and increasing neuronal excitability via binding to cognate receptors on neuronal, glial and perivascular cells (6). Moreover, reactive microglia can produce cytokines as a secondary "mirror" response to peripheral inflammation, hence, activating localized neuroinflammation in the CNS despite the lack of peripheral cell infiltrates (reviewed in 7). Therefore, there is an essential need to delineate the effect of PBMC extravasation from other peripheral inflammatory mediators on seizure precipitation.

Induction of peripheral immunity in experimental models has typically focused on activating pattern-recognition receptors, namely Toll-like receptors (TLRs) and NOD-like receptor (NLRs) (8). While TLRs are localized to either the cellular or endosomal membranes, and sense extracellular danger signals, such as bacterial- and viral-derived particles (8), NLRs are found in the cytosol (8) and sense intracellular stressors, such as ion efflux or reactive oxygen species (9, 10). The synergistic interaction of TLR4 and NLR Family Pyrin Domain Containing 3 (NLRP3) receptors triggers the oligomerization of cytosolic multiprotein complexes known as inflammasomes (11, 12). Inflammasome formation by means of the TLR4-NLRP3 two-signal pathway mediates immune activation, particularly in PBMCs, as well as secretion of pro-inflammatory interleukin (IL) cytokines like IL-1β and IL-18 (12, 13). In this two-signal system, the initial priming signal (signal 1) requires TLR4 binding to an immunogenic ligand, e.g. the gram-negative bacterial-derived cell-wall component lipopolysaccharide (LPS) (14), which triggers the downstream nuclear factor-κB pathway leading to the synthesis of the precursor form of IL-1β (pro-IL-1β) (12). Further, LPS causes potassium (K^+) efflux (9). As a result, a drop of intracellular K^+ concentration (signal 2) stimulates NLRP3 to recruit apoptosis-associated speck-like protein containing a carboxy-terminal CARD (ASC) adaptor protein and the interleukin-1 converting enzyme Caspase-1, which is normally expressed in its inactive form, i.e. pro-Caspase-1 (12). Assembly formation of the NLRP3-ASC-Caspase-1 inflammasome complex (also known as NLRP3 inflammasome) catalyzes the proteolytic conversion of pro-Caspase-1 to active Caspase-1. Activation of Caspase-1 subsequently promotes the maturation and release of IL-1β and IL-18 (12). Of interest, in vivo systemic administration of LPS produced a lower seizure threshold and an increase of neuronal excitability (6), suggesting that peripheral stimulation of

TLR4 modulates seizure activity. Also, recent clinical studies posited that seizure propensity was directly proportional to peripheral cellular and humoral expression of NLRP3 and inflammasome downstream product IL-1β, respectively (15, 16). Nevertheless, there is no explanation to date of the fundamental underpinnings that lie between peripheral activation of the TLR4-NLRP3 two-signal pathway and enhanced seizure susceptibility, and whether the penetration of pro-inflammatory PBMCs through the blood-brain barrier could be involved in the process.

To test the hypothesis that PBMC extravasation following peripheral induction of NLRP3 inflammasomes could elicit pathophysiological changes in brain excitability, we developed a novel in vitro co-culture model, where we used the membrane interface method to reproduce the interaction of two-signal activated PBMCs with CNS tissue. To reduce cross-reacting immunization of different cell types, organotypic brain slices containing the hippocampus and overlying cortex (i.e. organotypic cortico-hippocampal brain slice cultures or OCHSCs) were cultured together with spleen-derived PBMCs from the same animal. We activated the inflammasome two-signal system required for IL-1β and IL-18 release in PBMCs by sequential treatment of LPS (signal 1) followed by Nigericin (signal 2) (9, 12, 14, 17). Using whole-cell electrophysiological recordings, we first investigated the impact of PBMC immunoreactivity on the excitability of neurons in vitro by recording cortical and hippocampal pyramidal neurons from OCHSCs co-cultured with untreated, LPS-primed, or LPS + Nigericin two-signal activated PBMCs. We found that adding two-signal activated PBMCs enhanced the excitability of both cortical and hippocampal pyramidal neurons. However, upon adding LPS-primed PBMCs, a similar hyperexcitable response was manifested only by hippocampal neurons. Moreover, we revealed that PBMC-induced pro-excitatory effects were mediated by occlusion of the 4-aminopyridine (4-AP) sensitive K^+ currents: A-type fast activating, fast inactivating current (I_A) and D-type fast activating, slowly inactivating current (I_D).

Next, we added PBMCs to the media where the membrane insert physically separates PBMCs from OCHSCs. The semi-permeable membrane mimics the blood-brain barrier by allowing PBMC-derived soluble factors -but not PBMCs- to diffuse into the brain slice. We identified marked differences between LPS + Nigericin activated and LPS-primed PBMCs when added to the media, where activated, but not primed, PBMCs induced I_A- and I_D-mediated hyperexcitability in hippocampal neurons. In addition to investigating neuronal intrinsic membrane properties, we examined the potential transduction of peripheral inflammatory signals from PBMCs to OCHSCs in both settings: PBMC-OCHSC co-cultures and PBMC media incubation, using immunohistochemical analysis of neuroinflammation markers. We showed that inflammasome formation elicited by PBMCs was detected only in OCHSC tissue that exhibited reduction in I_A and I_D. Finally, by selectively targeting Caspase-1 catalytic activation, we sought to elucidate whether the NLRP3 downstream effector Caspase-1 has a potential role in inflammation transduction between PBMCs and the CNS, and convincingly found that Caspase-1 activation results in enhancing neuronal excitability by diminishing 4-AP sensitive K^+ currents that dampen neuronal membrane excitability, namely I_A and I_D.

Overall, the work presented here illustrates that inflammasome activation in peripheral immune cells influences neuronal excitability in the brain through a previously unrecognized mechanism, i.e. Caspase-1 mediated the impairment of 4-AP sensitive K^+ currents, which in turn increases seizure susceptibility. Elucidating the key role of Caspase-1 in driving neuromodulatory dysfunction provides a potential cellular target for exploring therapeutic interventions to control seizures associated with systemic immune response.

Materials And Methods

Experimental animals

Sprague–Dawley rats purchased from Charles River Laboratories (St. Constant, Quebec, Canada) were used in all experiments. Measures were taken to minimize the number of animals used.

OCHSC preparation

Brain tissue was obtained from male rat pups at postnatal days 9 and 10 (P9/P10). Animals were decapitated, and the brain was immediately removed and immersed in ice-cold modified Hanks' Balanced Salt Solution (HBSS) optimized for slice preparation (slicing solution): GIBCO HBSS containing calcium (Ca^{2+}) and magnesium (Mg^{2+}) (ThermoFisher Sciences), supplemented with 30 mM glucose, and 0.5 mM kynurenic acid; the pH was adjusted to 7.3–7.4, and osmolarity to 310–315 mOsm/L. Under sterile conditions, brains were hemisected and submerged in liquid agarose: low melting point TopVision agarose (ThermoFisher Sciences) dissolved in slicing solution (2% weight/volume) pre-warmed at 37ºC. Once solidified, the brain-containing agarose block was mounted on a slicing stage with superglue and 350 µm coronal slices of the dorsal frontal brain were cut with a vibrating blade microtome VT-1000-S (Leica Microsystems). In this study we used slices that contained the dorsal hippocampus and the overlying cortex. Cortico-hippocampal slices were collected and transferred to a Petri dish containing slicing solution and incubated at 4ºC for 1-1.5 hours. Individual slices were placed on 12 mm porous (0.4 µm) Millicell membrane inserts (Millipore-Sigma) at an interface with culture medium (one slice per insert) in 24-well culture plates, and put inside a 5% CO_2 incubator at 34ºC. After 48 hours, OCHSCs were incubated with a cocktail of anti-mitotic drugs diluted in OCHSC culture medium to inhibit glial proliferation, which throughout the course of our experiments resulted in the majority of the slice returning to a resting ramified state by 4–5 days in vitro (DIV). The cocktail consisted of the following (in µg/mL): 1.5 cytosine-β-D-arabino-funanoside (Millipore-Sigma), 1.5 uridine (Millipore-Sigma), and 1.55-Fluro-2'-deoxyuridine (Millipore-Sigma). Fresh medium was added after 24 hours, and afterwards the medium was changed every 2 days till the end of the experiment. The composition of OCHSC culture medium was the following: 50% minimum essential medium (with 25 mM HEPES), 20% heat inactivated horse serum, 25% HBSS containing Ca^{2+} and Mg^{2+} 1 mM GlutaMAX, 0.5 mM L-ascorbic acid, 55 mM glucose, 50–100 U/mL Penicillin-Streptomycin; pH 7.3–7.4; 310–315 mOsm/L. All components of the culture medium were supplied by ThermoFisher Sciences.

PBMC isolation and culturing

In parallel with brain tissue extraction, the spleen was quickly harvested from the same animal and kept in cold phosphate buffered saline (PBS), pH 7.4. Under a laminar flow hood, the spleen was homogenized and placed on top of a 70 µm Falcon cell strainer (ThermoFisher Sciences). Splenocytes were washed through the strainer with cold PBS, and cells were centrifuged. Splenocytes were thereafter centrifuged at 300 × g for 5 min at room temperature throughout all experimental protocols. Cell pellet was resuspended in ACK lysing buffer and incubated for 5 min to osmotically lyse erythrocytes before adding 10 × volume of PBS to relieve the osmotic pressure. Subsequently, spleen-derived PBMCs were centrifuged, resuspended in culture medium at a confluency of 1-1.5 × 10^6 cells/mL in a T25 flask, and transferred to a 5% CO_2 incubator at 37ºC. At 3 DIV, PBMCs were passaged by aspirating the medium-suspended portion of cells, mainly lymphocytes, whereas adherent cells, mainly monocytes, were detached using 0.05% trypsin. After combining all PBMC cell types, cells were centrifuged, washed with PBS, and centrifuged again before being resuspended in PBMC culture medium. PBMCs from each animal were equally divided into multiple T25 flasks at a confluency of 1-1.5 × 10^6 cells/mL and transferred to a 5% CO_2 incubator at 37ºC. The composition of PBMC culture medium was the following: 80% high glucose Dulbecco's modified eagle medium, 10% fetal bovine serum, 1% non-essential amino-acids, 1 mM sodium pyruvate, 2 mM L-glutamine, 50 µM β-mercaptophenol, 50–100 U/mL Penicillin-Streptomycin; pH 7.3–7.4. All reagents were obtained from ThermoFisher Sciences.

PBMC activation and co-culturing with OCHSCs

In the established protocol of TLR4-NLRP3 two-signal pathway activation (9, 12, 14), TL4 stimulation (signal 1) is conditional for prompting NLRP3 oligomerization (signal 2).Therefore, both signals 1 and 2 were sequentially induced at 6 DIV by first adding the TL4 ligand LPS (Escherichia coli serotype 0111: B4; Millipore-Sigma) at a concentration of 1 µg/ml to PBMCs in T25 flasks, and 3-3.5 hours later, 10 µM of the K^+ ionophore Nigericin (InvivoGen) was added to the LPS-treated flasks for 2.5-3 hours. In some cultures, PBMCs were incubated only with LPS for 3-3.5 hours without adding Nigericin, i.e. LPS-primed PBMCs (signal 1 only), and the rest of PBMC flasks were left untreated (naive PBMCs). Afterwards, immunogens were washed out by centrifugation, followed by resuspending the cell pellet in PBS, and washing all PBMC groups in OCHSC culture medium twice. Finally, PBMCs were collected by centrifugation. The PBMC-OCHSC co-culture system was established by seeding PBMCs on top of layer I of the cortex of OCHSCs at a concentration of ~ 3.0 × 10^4 cells per slice. For PBMC media incubation, ~ 9.0 × 10^4 cells were added to the media of OCHSCs. Slices derived from each animal were subdivided into one of the following experimental groups: naive OCHSCs, OCHSCs cultured with untreated PBMCs, OCHSCs cultured with LPS-primed PBMCs, and OCHSCs cultured with PBMCs activated by the incubation of LPS followed by Nigericin (LPS + Nigericin) (Fig. 1).

VX-765 Treatment

On 6 DIV, one hour prior to co-culturing PBMCs with OCHSCs, regular OCHSC medium was replaced with serum-free medium, which contains all components of the regular medium except for heat inactivated horse serum. The selective Caspase-1 inhibitor, VX-765 (or Belnacasan, MedChemExpress, stock

concentration 196.4 mM dissolved in DMSO) was added to serum-free medium at a final concentration of 100 µM, and 0.055% final DMSO volume. Concentration of VX-765 was selected based on an earlier study, which optimized the VX-765 dosage needed to inhibit NLRP3 inflammasome activation in organotypic hippocampal slice cultures (18). For control experiments, only the vehicle, i.e. DMSO, was added to the medium at the same volume. PBMC-OCHSC co-cultures were incubated with VX-765 overnight, and utilized for electrophysiology and immunohistochemistry experiments the next day, i.e. 7 DIV.

PBMC labeling with cell-tracing dye

For immunostaining experiments analyzing PBMC migration across OCHSCs, PBMCs were fluorescently labeled with the long-term cytoplasmic dye carboxyfluorescein diacetate succinimidyl ester (CFSE) as per the company's protocol (ThermoFisher Sciences) with some modifications (see below). At 6 DIV, PBMCs were aspirated and trypsinized as in the PBMC passaging protocol (see Sect. 3.3. PBMC isolation and culturing). After combining all PBMC cell types, cells were centrifuged, washed with PBS, and centrifuged again. Then, the supernatant was discarded, and cell pellet was resuspended in pre-warmed (37ºC) PBS. CellTrace far red CFSE dye (ThermoFisher Sciences) was added to PBMCs (1:5,000 dilution), and cells were incubated with the dye at 37ºC for 20 min. Afterwards, cells were centrifuged, and the pellet was washed with cold PBMC culture medium to washout unbound dye, followed by centrifugation. The pellet was resuspended in warm PBMC culture medium (with 20% fetal bovine serum), and cells were incubated at 37ºC for 5–10 min to activate the dye. Finally, cells were washed with OCHSC culture medium, the pellet was collected by centrifugation, and PBMCs were seeded either on top of OCHSCs or into OCHSC medium as above. After 2 hours, slices were fixed for 2 hours at 4 °C in 4% paraformaldehyde in PBS, pH 7.4, washed three times with PBS for 10 minutes, and mounted with Vectashield (Vector Labs). No antibodies were used for imaging of fluorescent $CFSE^+$ PBMCs.

Electrophysiology

Patch-clamp electrophysiological recordings in the whole-cell configuration were conducted between 7–11 DIV. On the day of the recording, individual slices were removed from the incubator, placed into a recording chamber, and continuously perfused with a pre-warmed (33 ± 1ºC) carbogenated artificial cerebrospinal fluid (ACSF) at a rate of 2–3 mL/min, which contained the following (in mM): 124 NaCl, 3 KCl, 1.3 $MgSO_4$-H_2O, 1.4 NaH_2PO_4, 10 D-glucose, 26 $NaHCO_3$ and 2.5 $CaCl_2$ (pH 7.3–7.4; 320–325 mOsm/L). Based on cell morphology and the presence of a large apical dendrite, layer II/III cortical and CA1 hippocampal pyramidal cells were visually identified with an upright microscope (Olympus) attached to a differential interference contrast optics and infrared video camera (Hitachi Kokusai Electric). Recording pipettes were pulled from borosilicate glass (World Precision Instruments) with a PP-83 two-stage puller (Narishige) to a resistance range of 5–7 MΩ when backfilled with intracellular solution containing (in mM): 129 K-gluconate, 10 HEPES, 5 KCl, 5 MgATP, 0.3 NaGTP, 1 EGTA and 0.3 $CaCl_2$. The pH and osmolarity were adjusted to 7.20–7.25 with KOH, and 300–305 mOsm/L, respectively. Biocytine (0.05–0.1%) was added to the intracellular solution for post-hoc confirmation of cell identity. Upon formation of a tight seal (> 1 GΩ) on pyramidal cell bodies, whole-cell configuration was achieved

by rupturing the membrane with negative pressure. Cell recordings were amplified and low-pass filtered at 1 kHz using Axopatch 200B amplifier (Molecular Devices), digitized with a Digidata 1440A analog-digital converter (Molecular Devices), and signals were acquired at a sampling rate of 10 kHz using the pCLAMP software 10.4 (Molecular Devices).

Once the whole-cell configuration was established, neurons were held at -60 mV for 4–6 min in voltage-clamp before experimental recordings. Neurons were only included in the analysis if they have shown stable (< 15%) holding current and access resistance in voltage-clamp throughout recording. Recordings of neuronal properties were made in voltage-clamp and current-clamp in normal ACSF and ≥ 5 min after drugs application to ACSF. Neuronal resting membrane potential was measured by averaging the potential over a 1 min period of passive recording in current-clamp. Rheobase, which is the minimum current required to elicit an action potential, was measured in current clamp with no holding current applied by injecting successive sweeps of incremental depolarizing current ramps at 100 pA per sweep. Repolarization time was measured as the outward current during the repolarization phase of the action potential, i.e. between the peak of the action potential and the trough after the action potential. Correction for liquid junction potential (~ + 14 mV) was not taken into consideration during these experiments.

To determine the amplitude of 4-AP sensitive K^+ currents I_A and I_D, cell output was measured in response to incremental successive voltage steps in the voltage-clamp configuration. 4-AP sensitive currents were isolated by adding 1 µM of the sodium (Na^+) current blocker tetrodotoxin (Tocris), 10 mM of the slow activating, non-inactivating K^+ current blocker tetraethylammonium chloride (Millipore-Sigma), and 0.5 mM of the non-selective Ca^{2+} current blocker nickel (II) chloride (Millipore-Sigma), to ACSF (baseline conditions). Since I_A and I_D have different sensitivities to 4-AP, 3 mM of 4-AP (Tocris) was added to block I_A and 40 µM of 4-AP was added to block I_D. 4-AP was perfused along with the abovementioned baseline channel inhibitors, then current response from the same cell was recorded. Change in net I_A and I_D currents was calculated by subtracting current values in the respective presence of 3 mM and 40 µM 4-AP from values during baseline conditions. For each voltage input step, current recordings were repeated a minimum of three times, and average output values were plotted versus voltage inputs to generate current-voltage (I-V) graphs.

Immunohistochemistry

All OCHSCs used for immunohistochemistry were collected at 7 DIV. In brief, slices were fixed for 2 hours at 4 °C in 4% paraformaldehyde in PBS, pH 7.4, washed three times with PBS for 10 minutes, then cryoprotected in 30% sucrose solution in PBS. Slices were blocked in 10% normal goat serum and 1% Triton X-100 in 1 × TBS (50 mM Tris–HCl, 150 mM NaCl, pH 7.4) for 2 hours at room temperature, and then incubated overnight at 4 °C in 10% normal goat serum, 0.3% Triton X-100 and primary antibodies diluted in 1 × TBS. Next, slices were washed three times in 1 × TBST (0.3% Triton X-100 in 1 × TBS) for 10 minutes, then incubated with secondary antibodies diluted in 1 × TBST for 2 hours at room temperature, before washing the slices again three times with 1 × TBST for 10 minutes. Finally, 4',6-diamidino-2-phenylindole (DAPI) (Millipore-Sigma) diluted in 1 × TBST (1/10,000) was applied for 5 minutes, then the

slices were washed three times in 1 × TBST for 10 minutes and mounted with Vectashield (Vector Labs). The following primary antibodies were used: mouse anti-ASC (1:250; Cat. No. sc-514414, Santa Cruz), mouse anti-NeuN (1:250; Cat. No. MAB377, Millipore-Sigma), rabbit anti-NLRP1 (1:1,000; Cat. No. 4990, Cell Signaling), rabbit anti-NLRP3 (1:500; Cat. No. LS-C334192, LifeSpan Biosciences). In addition, the following secondary antibodies were used: Alexa 488- and 594-conjugated goat IgG (1: 1,000; Molecular Probes).

Confocal microscopy

All imaging was performed on Leica Confocal microscope (LEICA TCS SP8) equipped with a motorized x–y–z stage control. Non-overlapping images from a single confocal plane were acquired with 20x (NA 0.75) and oil-immersion 63x (NA 1.40) objectives. The appropriate excitation wavelengths for blue (DAPI), green (Alexa-Fluor 488) and red (Alexa-Fluor 594) channels were used in a sequential order to eliminate any potential cross-talk, especially when imaging two or more channels. Scans from each channel were collected and subsequently merged. Images for individual antibodies (for example Nlrp1, Nlrp3 and ASC) were acquired using the same acquisition parameters. Bright-field images were taken in transmitted brightfield illumination. Since microglia close to the slice surface can remain in the activated state up to 6 DIV (19), we excluded the upper 50 µm of OCHSC tissue, and only the central zone of the slice was included in the analysis.

Experimental design and statistical analysis

Slices obtained from each animal were divided into different experimental groups, with each group being randomly assigned 1–2 slices. Electrophysiological data was analyzed using Clampfit 10.4 (Molecular Devices). Only one neuron per slice was recorded and included in the analysis. Statistics and graphs were produced using GraphPad Prism 5.0 (GraphPad Software). Normality of data distribution was assessed with D'Agostino & Pearson test. Differences between three or more experimental groups were assessed with one-way ANOVA followed by Bonferroni post hoc comparison. I_D and I_A differences were determined between three or more groups by repeated measures one-way ANOVA followed by Bonferroni post hoc comparison. All results are expressed as mean ± standard error of mean (SEM), with n being the number of neurons analyzed. Mean differences were considered to be significant at $p < 0.05$. Schematic illustrations were created with BioRender online platform (https://biorender.com).

Results

Direct contact between PBMCs and OCHSC cortical tissue triggers PBMC motility and allows translocation through cortical layers to the hippocampus

To identify potential inflammatory effects of PBMCs on cortical and hippocampal cells, OCHSCs from individual rats were co-cultured with PBMCs extracted from the same animal. Before adding PBMCs to OCHSCs, we incubated PBMCs with the specific TLR4 ligand LPS (signal 1) (14), followed by treatment

with the fungal-derived ionophore Nigericin, which induces K^+ efflux (signal 2) to activate NLRP3 (9, 14), therefore, giving rise to NLRP3 inflammasome. PBMCs were divided into three groups: 1) PBMCs stimulated by sequential incubation of LPS and Nigericin, hereafter referred to as immunoreactive PBMCs (IR-PBMCs), 2) primed PBMCs stimulated by LPS only (LPS-PBMCs), and untreated PBMCs (control PBMCs). OCHSC-PBMC co-culture groups were compared to naive OCHSCs (Fig. 1). Since different peripheral cell types can penetrate the blood-brain barrier and have the capacity to induce neuroinflammation upon extravasation (4, 5, 20, 21), we opted to include all splenic PBMC subtypes in our study rather than using a subset of purified cell types.

We first investigated the efficacy of the OCHSC-PBMC co-culture model by evaluating potential PBMC invasion of cortical and hippocampal layers upon seeding of PBMCs on top of cortical layer I of OCHSCs. Using pre-labeled control PBMCs with the fluorescent CFSE dye, we traced transmigration of PBMCs 2 hours after seeding them onto OCHSCs (Fig. 2). Transmigration of CFSE-labeled ($CFSE^+$) cells was detected throughout the entire slice, spreading across different cortical (Fig. 2C and E), and hippocampal layers (Fig. 2C and F). Further, localization of PBMCs was not limited to superficial sections of OCHSCs, but cells were also found in deep tissue sections irrespective to the OCHSC region, thus, suggestive of the formation of cell-adhesion between PBMCs and neural cells.

We next exploited the semi-porous properties of the membrane insert, which is at an interface between OCHSCs and culture media, to assess the effect of cytokine infiltration on neuronal function independently from PBMC trafficking. We compared a) adding $CFSE^+$ PBMCs on top of OCHSCs, where PBMCs are in direct contact with brain-derived tissue, to b) wherein $CFSE^+$ PBMCs were added solely to the media. In contrast to OCHSC-PBMC direct co-culture, no fluorescent cells were observed in OCHSCs when PBMCs were added to the media (Fig. 2D, G and H), thus showing that the membrane is impervious to PBMCs, and appears to effectively recapitulate some aspects of the blood-brain barrier by protecting OCHSCs from PBMC infiltration.

These findings denote that PBMCs retain their motility in vitro, with the capacity to crawl towards the cortex and the hippocampus upon the establishment of cell-cell contact between themselves and OCHSC tissue. Moreover, when PBMCs are applied to the media, the semi-porous membrane acts as a physical barrier isolating OCHSCs from PBMCs.

The hippocampus is more susceptible to PBMC-induced NLRP1 neuroinflammation than the cortex

PBMCs can transduce peripheral inflammatory signals to the CNS via secretory pro-inflammatory cytokines, such as IL-1β and IL-18, which can trigger neuroinflammation by binding to cognate receptors on the surface of neuronal and glial cells (e.g. IL-1R1 and IL-1R5) (17). Since exposure to both LPS and Nigericin is required for activation of the interleukin-1 converting enzyme Caspase-1 (11, 12, 14), pro-inflammatory cytokine release should be restricted to the two-signal activated IR-PBMCs, whereas LPS-PBMCs (signal 1 only) and control PBMCs, lack the capacity for cytokine production.

To verify potential cytokine-mediated transduction of peripheral inflammasomes to neural tissue when PBMCs come into close proximity with OCHSCs, we used immunohistochemical analysis to detect the expression profile of inflammasome markers, such as NLRP1 and NLRP3, in cortical and hippocampal OCHSC tissue. Immunolabeling of NLRP1 revealed that adding IR-PBMCs to OCHSCs resulted in NLRP1 induction in both cortical (Fig. 3J) and hippocampal cells (Fig. 4J) compared to naive OCHSCs (cortex, Fig. 3A; hippocampus, Fig. 4A). Surprisingly, following the administration of LPS-PBMCs, NLRP1 seems to be upregulated in the hippocampus (Fig. 4G), but not in the cortex (Fig. 3G) of OCHSCs, suggesting that immunologically primed PBMCs are capable of transducing peripheral inflammation to hippocampal cells. Conversely, NLRP1 was absent in the cortex (Fig. 3D) and hippocampus (Fig. 4D) of OCHSCs co-cultured with control PBMCs.

Next, we analyzed NLRP3 expression in OCHSCs. Similar to NLRP1 immunostaining results, NLRP3 immunoreactive cells were noted in the cortex (Fig. 3K) and the hippocampus (Fig. 4K) of IR-PBMC-OCHSC co-cultures. However, NLRP3 was upregulated in both the hippocampus (Fig. 4H) and the cortex (Fig. 3H) of LPS-PBMC-OCHSC co-cultures as opposed to naive OCHSCs (cortex, Fig. 3B; hippocampus, Fig. 4B). Thus, unlike NLRP1 inflammasomes, peripheral NLRP3 inflammasomes appear to be transduced to hippocampal as well as cortical cells in the LPS-PBMC group. On the other hand, NLRP3 was neither detectable in the cortex (Fig. 3E) nor in the hippocampus (Fig. 4E) when control PBMCs were added to OCHSCs.

A signature aspect of NLRP1 and NLRP3 inflammasome assembly and maturation is activation of the downstream effector ASC (22), however, NLRP1 can also promote inflammasome assembly independent of ASC (23). Therefore, we next investigated potential enhancement of ASC synthesis in OCHSCs following LPS- and IR-PBMCs application to OCHSCs. ASC seemed to be elevated in both the cortex and the hippocampus upon co-culturing OCHSCs with LPS-PBMCs (cortex, Figs. 3I and I´; hippocampus, 4I and I´) and IR-PBMCs (cortex, Figs. 3L and L´; hippocampus, 4L and L´) as compared to the cortex and hippocampus of control PBMC-OCHSC co-cultures (cortex, Figs. 3F and F´; hippocampus, 4F and F´) and naive OCHSCs (cortex, Figs. 3C and C´; hippocampus, 4C and C´). Hence, ASC expression was only detected when NLRP3 was also expressed.

Altogether, analysis of inflammasome induction in OCHSCs indicates that signal 1 priming of PBMCs via LPS, irrespective of signal 2 activation, was sufficient to transduce peripheral pro-inflammatory signals to OCHSCs, which is manifested by the expression of NLRP3 inflammasome cascade, i.e. NLRP3 and ASC, in cortical and hippocampal cells. Nevertheless, while on the one hand, triggering of NLRP1 inflammasome in the hippocampus was elicited by LPS- and IR-PBMCs, on the other hand, NLRP1 expression in the cortex was induced by IR-PBMCs, but not LPS-PBMCs. This suggests that signal 2 - together with signal 1- activation is necessary to generate NLRP1 inflammasome in the cortex, whereas the hippocampus seems to be vulnerable to signal-1-mediated peripheral transduction of NLRP1 inflammasome. Additionally, adding control PBMCs to OCHSCs appears to be innocuous, as there was no NLRP1/3 inflammasome recruitment in either the cortex or the hippocampus.

Transduction of peripheral inflammation to neural tissue is coupled with hyperexcitability in pyramidal neurons

To address whether peripheral inflammasomes transduced to OCHSCs may give rise to functional changes in cortical and hippocampal neurons, we measured neuronal excitability by performing whole-cell electrophysiological recordings in pyramidal neurons in cortical layer II/III and in the CA1 region of the hippocampus.

Cortical pyramidal neurons from all experimental PBMC-OCHSC groups showed similar resting membrane potential values to naive OCHSCs (naive OCHSCs: -65.28 ± 6.87 mV, n = 11; control PBMCs: -68.52 ± 6.15 mV, n = 11; LPS-PBMCs: -65.25 ± 5.16 mV, n = 10; IR-PBMCs: -66.64 ± 6.75 mV, n = 10; p = 0.59; one-way ANOVA). Also, there was no change in cortical cell membrane capacitance (C_m) between OCHSCs incubated with all PBMC groups and naive OCHSCs (naive OCHSCs: 70.48 ± 13.54 pF, n = 11; control PBMCs: 70.40 ± 11.78 pF, n = 11; LPS-PBMCs: 73.04 ± 13.25 pF, n = 10; IR-PBMCs: 75.85 ± 7.55 pF, n = 10; p = 0.69; one-way ANOVA). In addition, no change in the duration of action potential repolarization (APR) was exhibited by cortical neurons in any of the PBMC-OCHSC co-cultures versus naive OCHSCs (IR-PBMCs: 2.02 ± 0.45 msec, n = 10; LPS-PBMCs: 2.11 ± 0.43 msec, n = 10; control PBMCs: 2.18 ± 0.38 msec, n = 11; naive OCHSCs: 2.07 ± 0.34 msec, n = 11; p = 0.82; one-way ANOVA) (Fig. 3Q and R). However, compared to naive OCHSCs, adding IR-PBMCs and LPS-PBMCs to OCHSCs significantly increased the input resistance (R_{in}) of cortical neurons, while there was no change after adding control PBMCs (naive OCHSCs: 140.35 ± 21.37 MΩ, n = 11, control PBMCs: 144.50 ± 30.92 MΩ, n = 11, p > 0.99, LPS-PBMCs: 174.20 ± 24.87 MΩ, n = 10, p < 0.05, IR-PBMCs: 180.65 ± 26.00 MΩ, n = 10, p < 0.01; one-way ANOVA). Increase of R_{in} manifested after adding IR-PBMCs was also significantly higher than that measured after adding control PBMCs (p < 0.05; one-way ANOVA) (Fig. 3M and N). Furthermore, while the rheobase of cortical neurons was significantly lower in the IR-PBMC-OCHSC co-culture group versus naive OCHSC and control PBMCs groups, the rheobase of cortical neurons after adding LPS-PBMCs and control PBMCs was comparable to those of naive OCHSCs (naive OCHSCs: 301.48 ± 119.33 pA, n = 11, control PBMCs: 282.36 ± 68.85 pA, n = 11; p > 0.99, LPS-PBMCs: 268.21 ± 70.90 pA, n = 10; p > 0.99, IR-PBMCs: 175.20 ± 69.12 pA, n = 10, p < 0.05 compared to naive OCHSCs, p < 0.05 compared to control PBMCs; one-way ANOVA) (Fig. 3O and P).

Hence, following the application of control, LPS- or IR-PBMCs, cortical neurons did not display noticeable electrophysiological alterations with respect to resting membrane potential, C_m or APR. Yet, co-culturing of LPS- and IR-PBMCs did induce R_{in} changes in cortical neurons. Interestingly, only the addition of IR-PBMCs produced changes in action potential firing propensity, i.e. rheobase, whereas the addition of LPS-primed PBMCs had no effect on cell firing.

Recordings from hippocampal pyramidal neurons were, for the most part, analogous to their cortical counterparts, since there were no notable differences between naive OCHSCs and OCHSCs co-cultured with any of the PBMC groups with respect to resting membrane potential (naive OCHSCs: -59.41 ±

3.47 mV, n = 23; control PBMCs: -59.73 ± 1.92 mV, n = 21; LPS-PBMCs: -58.85 ± 3.00 mV, n = 19; IR-PBMCs: -59.01 ± 2.49 mV, n = 20, p = 0.75; one-way ANOVA), or C_m (naive OCHSCs: 100.1 ± 20.53 pF, n = 23; control PBMCs: 100.4 ± 28.84 pF, n = 21; LPS-PBMCs: 90.69 ± 23.93 pF, n = 19; IR-PBMCs: 95.03 ± 18.44 pF, n = 20, p = 0.50; one-way ANOVA). Also, similar to cortical neurons, hippocampal neurons exhibited significantly augmented R_{in} after seeding of IR-PBMCs and LPS-PBMCs on OCHSCs relative to naive OCHSCs, and this augmentation was significant for both groups when compared to control PBMCs, which was not significantly different from naive OCHSCs (naive OCHSCs: 101.87 ± 9.07 MΩ, n = 23, control PBMCs: 101.87 ± 11.23 MΩ, n = 21, p > 0.99, LPS-PBMCs: 125.18 ± 11.60 MΩ, n = 19, p < 0.001 versus naive OCHSCs, p < 0.001 versus control PBMCs, IR-PBMCs: 121.46 ± 11.41 MΩ, n = 20, p < 0.001 versus naive OCHSCs, p < 0.001 versus control PBMCs; one-way ANOVA) (Fig. 4M and N).

In terms of cell firing, application of IR-PBMCs to OCHSCs resulted in rheobase reduction versus control PBMCs and naive OCHSCs. Also, there was no significant difference between control PBMC-OCHSC co-cultures and naive OCHSC. Conversely, unlike cortical pyramidal neurons, following LPS-PBMCs application, the rheobase of hippocampal neurons was markedly reduced compared to control PBMCs and naive OCHSCs (naive OCHSCs: 261.77 ± 80.86 pA, control PBMCs: 261.01 ± 46.13 pA, n = 21, p > 0.99, LPS-PBMCs: 194.92 ± 61.14 pA, n = 19, p < 0.01 versus naive OCHSCs, p < 0.01 versus control PBMCs, IR-PBMCs: 191.96 ± 48.96, n = 20, p < 0.01 versus naive OCHSCs, p < 0.01 versus control PBMCs; one-way ANOVA) (Fig. 4O and P). Thus, in contrast to the cortex, the effect of LPS-primed PBMCs on rheobase in the hippocampus was reminiscent to IR-PBMCs, eliciting hyperexcitability in OCHSCs co-cultured with LPS-PBMCs and IR-PBMCs versus the control groups.

Likewise, the repolarization phase was notably extended in hippocampal pyramidal neurons recorded following IR-PBMCs and LPS-PBMCs incubation, when compared to control PBMCs incubation and naive OCHSCs, with no significant change between naive OCHSCs and OCHSCs co-cultured with control PBMCs (naive OCHSCs: 1.31 ± 0.16 msec, n = 15, control PBMCs: 1.29 ± 0.20 msec, n = 15, p > 0.99, LPS-PBMCs: 1.53 ± 0.20 msec, n = 15, p < 0.05 versus naive OCHSCs, p < 0.05 versus control PBMCs, IR-PBMCs: 1.52 ± 0.20 msec, n = 15, p < 0.05 versus naive OCHSCs, p < 0.01 versus control PBMCs; one-way ANOVA) (Fig. 4Q and R). Accordingly, unlike the cortex where none of the PBMC groups had an effect on APR, LPS- and IR-PBMCs generated extended APR in hippocampal neurons, suggestive of different action potential kinetics between cortical and hippocampal neurons.

Taken together, upon application on OCHSCs, both LPS- and IR-PBMCs altered some of the intrinsic properties of cortical and hippocampal pyramidal neurons associated with excitability. Notably, enhancement of neuronal excitability appears to be concomitant with the expression of NLRP1 and/or NLRP3 inflammatory markers in OCHSCs.

Activation of inflammasomes in OCHSCs promotes a decline in 4-AP sensitive transient K^+ currents in pyramidal

neurons

Reduction of rheobase and prolongation of the repolarization duration in pyramidal neurons after exposure to PBMCs is likely to arise from changes in the properties of specific ion channels that are activated when graded potential reaches threshold potential as well as during the repolarization phase. Thus, we next asked which ion channels would satisfy these criteria.

Interestingly, transient A-type fast activating, fast inactivating voltage-dependent K^+ current (I_A) is known to regulate action potential rheobase and waveform (24–26). In addition, LPS incubation with caudate nucleus cultures has been shown to reduce I_A in vitro (27). Therefore, we postulated that suppression of I_A might be a plausible culprit underlying neuronal excitability changes elicited by inflammation. To explore putative suppression of I_A in OCHSCs, we selectively inhibited I_A by adding 3 mM of 4-AP during recording of pyramidal neurons. Our approach was to distinguish I_A from other currents initiated at threshold potential and activated throughout different action potential phases. Hence, we obtained whole-cell recordings while blocking Na^+, Ca^{2+} currents together with the majority of K^+ currents (also referred to as baseline conditions), then repeated the same recordings again while adding 4-AP to the abovementioned current blockers, and derived net I_A by calculating current difference between both conditions.

I_A in cortical neurons was notably abrogated in the IR-PBMCs group versus naive OCHSCs and control PBMCs groups, whereas cortical neurons in the LPS-PBMCs and control PBMCs groups showed similar I_A activation to naive OCHSCs (current response at + 20 mV, i.e. maximum voltage input, naive OCHSCs: 897.53 ± 87.52 pA, n = 6, control PBMCs: 972.12 ± 129.91 pA, n = 6, $p > 0.99$, LPS-PBMCs: 791.12 ± 116.90 pA, n = 6, $p = 0.82$, IR-PBMCs: 515.81 ± 58.65 pA, n = 6, $p < 0.01$ versus naive OCHSCs, $p < 0.001$ versus control PBMCs, repeated measures one-way ANOVA) (Fig. 5A, B and E). On the other hand, adding either IR-PBMCs or LPS-PBMCs to OCHSCs substantially reduced I_A in hippocampal neurons relative to naive OCHSCs and to control PBMCs. Markedly, the effect of co-culturing control PBMCs with OCHSCs was opposite to LPS- and IR-PBMCs, resulting in potentiation of I_A amplitude compared to naive OCHSCs (current response at + 20 mV, naive OCHSCs: 928.82 ± 83.55 pA, n = 7, control PBMCs: 930.35 ± 145.81 pA, n = 6, $p < 0.0001$, LPS-PBMCs: 648.57 ± 111.67 pA, n = 6, $p < 0.0001$ versus naive OCHSCs, $p < 0.0001$ versus control PBMCs, IR-PBMCs: 617.99 ± 52.41 pA, n = 6, $p < 0.001$ versus naive OCHSCs, $p < 0.0001$ versus control PBMCs, repeated measures one-way ANOVA) (Fig. 5C, D and G).

Beside I_A, we also considered other potential ion channel candidates influenced by PBMC-induced neuroinflammation. Given that transient D-type fast activating, slowly inactivating voltage-dependent K^+ current (I_D) is sensitive to 4-AP much like I_A, and activation of I_D delays action potential firing along with reducing action potential duration in pyramidal neurons (24, 26, 28, 29), we decided to investigate the possible contribution of I_D in inflammation-induced excitability. However, while 4-AP inhibits I_A activation in millimolar concentrations, (1–3 mM), I_D is highly sensitive to 4-AP, i.e. in micromolar concentrations

(30–100 μM) (24–26, 28). Therefore, we isolated I_D using the same approach as I_A, except the concentration of 4-AP was 40 μM, instead of 3 mM.

Results from pyramidal neurons in the cortex revealed that relative to naive OCHSCs, the amplitude of I_D was significantly diminished only in the IR-PBMCs co-cultured with OCHSCs, whereas there were no notable changes in I_D amplitude upon co-culturing control PBMCs or LPS-PBMCs with OCHSCs (current response at + 20 mV, naive OCHSCs: 256.25 ± 15.01, n = 9, control PBMCs: 226.92 ± 10.84 pA, n = 8, p = 0.08, LPS-PBMCs: 206.64 ± 24.01 pA, n = 9, p = 0.35, IR-PBMCs: 175.03 ± 23.88 pA, n = 9, p < 0.01, repeated measures one-way ANOVA) (Fig. 5H, I and L). In hippocampal neurons, OCHSCs co-cultured with IR-PBMCs and LPS-PBMCs manifested significantly lower I_D than naive OCHSCs as well as control PBMC-OCHSC co-cultures, whereas adding control PBMCs did not result in significant changes in I_D compared to naive OCHSCs (current response at + 20 mV, naive OCHSCs: 253.39 ± 21.49 pA, n = 11, control PBMCs: 229.38 ± 20.04 pA, n = 12, p = 0.06, LPS-PBMCs: 161.32 ± 15.81 pA, n = 12, p < 0.0001 versus naive OCHSCs, p < 0.001 versus control PBMCs, IR-PBMCs: 155.66 ± 15.74 pA, n = 11, p < 0.0001 versus naive OCHSCs, p < 0.0001 versus control PBMCs, repeated measures one-way ANOVA) (Fig. 5J, K and N).

Collectively, changes in I_A and I_D are in line with our previous data, where decay of I_A and I_D was only detected in pyramidal neurons that exhibited changes in cell firing associated with inflammasome induction, i.e. the cortex of IR-PBMC-OCHSC co-cultures and the hippocampus of IR-PBMC- and LPS-PBMC-OCHSC co-cultures. Thus, transduction of peripheral inflammation to OCHSCs leads to a decrease in the amplitude of I_A and I_D, which consequently promotes hyperexcitability in pyramidal neurons.

Direct cell-cell contact between PBMCs and OCHSCs is required for pro-inflammatory signal transduction from LPS-primed PBMCs to brain-derived tissue

To gain further insight into how pro-inflammatory PBMCs can transduce peripheral inflammation to OCHSCs, we investigated whether diffusible factors secreted by PBMCs, primarily cytokines and chemokines, can mediate inflammasome transduction solely by binding to their cognate receptors found in OCHSC cells (17). Since we have demonstrated that when PBMCs were added to the media, the membrane insert acts as a barrier by preventing cell-cell adhesion between PBMCs and OCHSCs (see Sect. 4.1), we decided to add PBMCs to OCHSC media, where presumably PBMC-derived cytokines and chemokines, but not PBMCs themselves, can diffuse through the membrane. To inquire whether the outcome of adding PBMCs to OCHSC media would mimic that of co-culturing PBMCs in direct contact with OCHSCs, we examined potential expression of NLRP1 and NLRP3 inflammasome markers along with potential changes in excitability parameters and 4-AP sensitive currents after adding control PBMCs, LPS-PBMCs and IR-PBMCs to the media. In the next set of experiments, we only investigated the effects of media-incubated PBMCs on the hippocampus because the hippocampus was more susceptible to PBMC-induced hyperexcitability than the cortex.

Our immunohistochemical analysis of the inflammasome markers NLRP1, NLPR3 and the downstream effector ASC in OCHSCs revealed that media incubation of IR-PBMCs (mIR-PBMCs) gave rise to the upregulation of NLRP1 (Fig. 6G), NLRP3 (Fig. 6H) and ASC (Fig. 6I and I´) in the hippocampus. However, there was no detectable expression of NLRP1, NLRP3 or ASC following media incubation of LPS-PBMCs (mLPS-PBMCs) (Fig. 6D-F´) as compared to control PBMCs (mCTL-PBMCs) (Fig. 6A-C´). The presence of inflammasomes in the mIR-PBMCs group supports the notion that IR-PBMCs can transduce inflammation through diffusible cytokines, whereas failure of mLPS-PBMCs to evoke similar effect suggests that LPS-PBMCs require cell-cell contact for inflammation transduction.

Also, following media incubation of all experimental PBMC groups, the values of R_{in}, rheobase and APR in hippocampal pyramidal neurons exposed to mLPS-PBMCs were reminiscent to hippocampal neurons exposed to mCTL-PBMCs, and consistent with the absence of hippocampal inflammation in OCHSCs following mLPS-PBMCs. However, in hippocampal neurons exposed to mIR-PBMCs, R_{in}, rheobase and APR values were significantly different from mCTL-PBMCs, again consistent with inflammasome induction in OCHSCs from this group (R_{in}, mCTL-PBMCs: 109.30 ± 12.98 MΩ, n = 11, mLPS-PBMCs: 117.78 ± 15.50 MΩ, n = 11, p = 0.41, mIR-PBMCs: 127.51 ± 9.64 MΩ, n = 10, p < 0.01; rheobase, mCTL-PBMCs: 212.63 ± 46.88 pA, mLPS-PBMCs: 192.86 ± 36.64 pA, n = 11, p = 0.93, mIR-PBMCs: 155.55 ± 50.95 pA, n = 10, p < 0.05; APR, mCTL-PBMCs: 1.31 ± 0.14 msec, n = 11, mLPS-PBMCs: 1.36 ± 0.17 msec, n = 11, p > 0.99, mIR-PBMCs: 1.52 ± 0.20 msec, n = 10, p < 0.05; one-way ANOVA) (Fig. 6J-L). Hence, in contrast to adding LPS-PBMCs on top of OCHSCs (Sect. 4.3, Fig. 4G-I´ and M-R), the outcome of mLPS-PBMCs was comparable to that of mCTL-PBMCs, indicating that media application of LPS-PBMCs occludes their influence on neuronal excitability. Importantly, mIR-PBMCs retained their capacity to trigger neuroinflammation and enhance neuronal excitability, suggesting that diffusion of inflammatory factors secreted by mIR-PBMCs, likely cytokines, rather than cell-cell contact is responsible of the phenotypic changes observed in OCHSCs.

Furthermore, the difference of the amplitude of the 4-AP sensitive I_A and I_D between hippocampal neurons of OCHSCs incubated with mLPS-PBMCs and those incubated with mCTL-PBMCs was not significant. Still, both I_A and I_D amplitudes were significantly lower in hippocampal neurons when OCHSCs were incubated with mIR-PBMCs as opposed to those incubated with mCTL-PBMCs and mLPS-PBMCs (current response at + 20 mV, I_A, mCTL-PBMCs: 1178.43 ± 119.61 pA, n = 6, mLPS-PBMCs: 1100.72 ± 45.87 pA, n = 5, p > 0.99, mIR-PBMCs: 855.10 ± 66.09 pA, n = 5, p < 0.01 versus mCTL-PBMCs, p < 0.01 versus mLPS-PBMCs; I_D, mCTL-PBMCs: 254.20 ± 27.69 pA, n = 8, mLPS-PBMCs: 280.10 ± 20.16 pA, n = 8, p > 0.99, mIR-PBMCs: 160.48 ± 25.92 pA, n = 7, p < 0.05 versus mCTL-PBMCs, p < 0.01 versus mLPS-PBMCs; repeated measures one-way ANOVA) (Fig. 6M-Q). The fact that significant decrease of amplitude of I_A and I_D was present only in the mIR-PBMCs group further confirms the correlation between PBMC-induced hyperexcitability and changes in these 4-AP sensitive currents.

In essence, with respect to the hippocampus, mIR-PBMCs replicated the effects of co-culturing IR-PBMCs with OCHSCs, reproducing neuroinflammation and I_D-/I_A-mediated hyperexcitability. On the contrary,

mLPS-PBMCs unexpectedly failed to provoke neuroinflammation or neuronal hyperexcitability unlike LPS-PBMC-OCHSC co-cultures. Thus, our data shows that in the case of IR-PBMCs, cell-cell contact between PBMCs and OCHSCs is not necessary to yield neuroinflammation in OCHSC hippocampal cells, thereby suggesting that PBMC-derived pro-inflammatory cytokines are potential mediators of peripheral inflammatory transduction. Nevertheless, cell-cell contact seems to be essential for transducing peripheral inflammasomes from LPS-PBMCs to the hippocampus in OCHSCs, underscoring the possibility that PBMC binding to an antigen enriched in the hippocampus is necessary for immunologically-primed PBMCs to become immunologically-activated (see Discussion).

Neuroinflammation-mediated attenuation of 4-AP sensitive transient K^+ currents is dependent on Caspase-1 activation in hippocampal cells

A key regulatory step in the oligomerization of Caspase-1-activating inflammasome complexes is the cleavage of the precursor form of Caspase-1, i.e. pro-Caspase-1, into its activated form (12, 14, 22). Indeed, inhibiting Caspase-1 cleavage using the selective Caspase-1 inhibitor VX-765 has proved to be highly effective in reducing downstream activation of NLRP1 and NLRP3 inflammasomes in the CNS (30, 31).

To test if Caspase-1 inhibition could possibly mitigate PBMC-induced neuroinflammation in the hippocampus, OCHSCs were pre-treated with VX-765 one hour before seeding LPS-PBMCs and IR-PBMCs on top of OCHSCs. Thereafter, we looked into the profile expression of NLRP1 and NLRP3 inflammasome markers, and also measured excitability parameters (R_{in}, rheobase, APR) together with 4-AP sensitive currents following the co-culturing of LPS-PBMCs (VX765-LPS-PBMCs) and IR-PBMCs (VX765-IR-PBMCs) with OCHSCs. Because VX-765 was dissolved in DMSO, we pre-treated OCHSCs with DMSO, i.e. the vehicle, one hour prior to applying LPS-PBMCs (DMSO-LPS-PBMCs) and deemed this group as the positive control group.

We found augmented NLRP1, NLRP3 and ASC immunolabeling in the DMSO-LPS-PBMCs group (Fig. 7A-C´) as opposed to VX765-LPS-PBMCs (Fig. 7D-F´) and VX765-IR-PBMCs (Fig. 7G-I´). Thus, these observations implicate VX-765 as a potent inhibitor of PBMC-transduced inflammasomes in OCHSC hippocampal tissue.

In addition, patch-clamp recordings showed that hippocampal pyramidal neurons displayed significantly lower R_{in}, lower rheobase and slower APR in DMSO-LPS-PBMC co-cultures relative to VX765-LPS-PBMCs and VX765-IR-PBMC co-cultures (R_{in}, DMSO-LPS-PBMCs: 132.44 ± 20.12 MΩ, n = 9, VX765-LPS-PBMCs: 104.20 ± 19.07 MΩ, n = 9, $p < 0.01$, VX765-IR-PBMCs: 110.44 ± 13.91 MΩ, n = 9, $p < 0.05$; rheobase, DMSO-LPS-PBMCs: 173.29 ± 37.27 pA, n = 9, VX765-LPS-PBMCs: 268.52 ± 79.76 pA, n = 9, $p < 0.05$, VX765-IR-PBMCs: 281.13 ± 98.83 pA, n = 9, $p < 0.05$; APR, DMSO-LPS-PBMCs: 1.56 ± 0.20 msec, n = 9, VX765-LPS-PBMCs: 1.32 ± 0.16 msec, n = 9, $p < 0.05$,VX765-IR-PBMCs: 1.31 ± 0.17 msec, n = 9, $p < 0.05$; one-way

ANOVA) (Fig. 7J-L). Further, I_A and I_D amplitudes of hippocampal neurons from DMSO-LPS-PBMC co-cultures were notably reduced versus VX765-LPS-PBMCs and VX765-IR-PBMC co-cultures (current response at + 20 mV, I_A, DMSO-LPS-PBMCs: 747.64 ± 64.58 pA, n = 5, VX765-LPS-PBMCs: 1080.72 ± 52.84 pA, n = 5, $p < 0.001$, VX765-IR-PBMCs: 983.24 ± 97.73 pA, n = 5, $p < 0.01$; I_D, DMSO-LPS-PBMCs: 171.61 ± 11.41, n = 7, VX765-LPS-PBMCs: 266.99 ± 43.55 pA, n = 8, $p < 0.001$, VX765-IR-PBMCs: 236.95 ± 34.51 pA, n = 8, $p < 0.05$; repeated measures one-way ANOVA) (Fig. 7M-P). These electrophysiological findings were concordant with VX-765-induced suppression of peripheral inflammasome transduction to the hippocampus, and strongly suggest that I_A- and I_D-mediated hyperexcitability is caused by inflammasome formation.

Taken together, this data provides evidence that in the hippocampus, VX-765 treatment reversed the hyperexcitability concurrent with neuroinflammation triggered by pro-inflammatory PBMCs, therefore implicating Caspase-1–dependent pathway(s) as the main underlying mechanism of PBMC-induced I_A- and I_D-mediated enhanced excitability.

Discussion

Excessive or prolonged neuroinflammation in the CNS is a causal factor of many neurological disorders (32). Yet, induction of innate immunity outside of the CNS, i.e. peripheral inflammation, can also promote neuroinflammation, which may subsequently lead or contribute to pathophysiological disorders within the CNS, including epilepsy (1, 33). More recently, inflammasomes, through activation of Caspase-complexes, have been found to contribute to the initiation of innate immune response, including release of pro-inflammatory cytokines and pyroptotic cell death, (34), and a growing body of research suggests that inflammasomes may constitute potential therapeutic targets (35). In order to delineate the mechanisms that facilitate the propagation of peripheral inflammation to the brain following PBMC extravasation, in this study, we employed an established pharmacological approach to induce inflammasomes in PBMCs in vitro. Our approach exploited the well-characterized sequential incubation of the immunogens LPS and Nigericin to activate the two-signal pathway required for NLRP3 inflammasome formation (9, 12, 14). Therefore, we co-cultured PBMCs with OCHSCs derived from the same animal and used inflammasome-activated IR-PBMCs and primed LPS-PBMCs to study potential transduction of peripheral inflammasomes to the CNS. Further, we compared both types of stimulated PBMCs with naive PBMCs that were not exposed to immunogens. Overall, the data presented herein demonstrates that triggering inflammasomes in PBMCs results in neuronal hyperexcitability upon PBMC encounter with CNS tissue, thus, suggesting that inflammasome activation in peripheral immune cells has pathogenic implications on the brain. A second significant finding here is that the hippocampus is more prone to the pro-excitant effects of systemic inflammation than the cortex. In addition, we provide new evidence that I_A and I_D are downstream targets of Caspase-1-activating inflammasomes. Indeed, our results showing that Caspase-1 activation diminishes I_A and I_D raise the possibility that aberrant functional changes of 4-AP sensitive K^+ currents induced by inflammasome formation contribute to the previously reported proconvulsant effects of Caspase-1 (36–38).

Using the PBMC-OCHSC co-culture model in conjunction with fluorescent live-cell labeling of PBMCs, we revealed that naive PBMCs have the capacity to adhere to OCHSCs, which denote potential immunological crosstalk between PBMCs and neural cells. Yet, because the fluorescent dye used was not specific to certain PBMC subpopulations, we could not identify whether cell-cell contact was established between all or only some peripheral cell subtypes and brain-derived tissue. Future studies should unveil the identity of neuronal/glial cells and PBMC subtypes that establish cell-cell adhesion in our model. In contrast, adding PBMCs solely to the media failed to result in PBMC adherence to OCHSC tissue as the membrane inset prevented infiltration of media-incubated PBMCs. This attribute of the interface culture system allowed us to compare the outcome of culturing inflammatory PBMCs in direct contact with OCHSCs, with that of culturing inflammatory PBMCs in the media in isolation from OCHSCs, in our studies.

When PBMCs were co-cultured in direct contact with OCHSCs, there were evident differences between the cortex and the hippocampus. Both LPS-PBMCs and IR-PBMCs triggered NLRP3 formation in cortical and hippocampal tissues when co-cultured with OCHSCs. While IR-PBMCs induced NLRP1 expression in the cortex and the hippocampus, LPS-PBMCs induced NLRP1 expression only in the hippocampus. Furthermore, there were profound differences between the cortex and the hippocampus with respect to neuronal excitability. Adding IR-PBMCs to OCHSCs resulted in pro-excitable changes in R_{in}, rheobase, I_A and I_D in cortical and hippocampal pyramidal neurons. However, IR-PBMCs induced APR extension only in the hippocampus but not in the cortex, which could be attributed to a difference in the channel types contributing to the total hyperpolarizing current during the repolarization phase between the cortex and the hippocampus (see below). On the other hand, adding LPS-PBMCs to OCHSCs produced disparate outcomes in excitability between the cortex and the hippocampus, with hippocampal neurons exhibiting pro-excitatory changes reminiscent to adding IR-PBMCs, whereas there were no significant changes observed in cortical neurons in any of the investigated excitability parameters except for elevation in R_{in}. Thus, the hippocampus was more vulnerable to co-culturing of LPS-PBMCs than the cortex, since in addition to NLRP3 inflammasome generation and R_{in} changes seen in the cortex, the hippocampus also displayed NLRP1 induction together with lower rheobase, I_A and I_D. Interestingly, a previous report also found that systemic administration of LPS in vivo rendered the hippocampus more susceptible to neuroinflammation than the cortex (39). One explanation of this phenomenon could be ascribed to the relatively high expression of IL-1 receptors in the hippocampus, specifically the dentate gyrus, compared to other structures like the cortex, which leads to higher sensitivity to IL-1 cytokines, including IL-1β (40–42). Notably, untreated PBMCs failed to induce neuroinflammation. This finding is corroborated by a previous report indicating that lymph-node-derived lymphocytes not only failed to give rise to neuroinflammation when incubated with brain-derived organotypic slices in vitro, but they were neuroprotective against neurotoxicity (43).

It was previously shown that infiltration of peripheral monocyte-derived macrophages into the CNS enhances glutamate-induced excitotoxicity in neurons (44, 45). However, there are conflicting reports on whether extravasation of T-lymphocytes leads to augmentation (46) or suppression (47) of neuronal

network excitability. Also, it is noteworthy to mention that a recent report identified opposing effects of different T-lymphocyte subpopulations subsequent to leukocyte extravasation, where γδ T-lymphocytes exacerbated seizures, while on the other hand, regulatory T-lymphocytes displayed anti-convulsant effects in an experimental epilepsy model (48). Thus, it will be important in future studies to determine whether either lymphocytic or myeloid cell subtypes isolated from PBMCs can mediate pathological pro-excitation of pyramidal neurons when co-cultured alone with OCHSCs. In the case of lymphocytic cells, it also needs to be determined whether CNS resident cells, such as microglia, can capture antigens to present to activated T-lymphocytes, i.e. act as resident antigen presenting cells, in the absence of myeloid antigen presenting cells, such as dendritic cells (49).

Adding IR-PBMCs to the media provoked neuroinflammation and hyperexcitability in hippocampal neurons in the same fashion as adding IR-PBMCs directly on top of OCHSCs. These results favor the notion that inflammatory transduction was achieved via binding of cytokines released by IR-PBMCs to their cognate receptors in the hippocampus. However, media application of LPS-PBMCs failed to either yield NLRP1/3 inflammasome activation or enhance neuronal excitability in the hippocampus, which indicates that transduction of peripheral inflammation to the hippocampus was dependent on the interaction of PBMCs with OCHSC cells. This cell-cell interaction requirement for LPS-PBMCs to transduce peripheral pro-inflammatory signals to OCHSCs suggests that LPS-PBMCs lack the capacity to secrete pro-inflammatory cytokines, which opens the question to how LPS-PBMCs added on top of OCHSCs promote inflammation in the hippocampus? Dulken et al. reported that T-lymphocyte infiltrates in the mouse brain have a much higher ability to clonally expand than T-lymphocytes in the bloodstream (50). This clonal expansion is a prominent feature of pro-inflammatory activation as well as subsequent cytokine release in T-lymphocytes. (50). These findings suggest that a specific antigen in the mouse brain recognized by brain-residing T-lymphocytes triggered a localized immune response. Therefore, it is conceivable that cell-cell contact formation between signal-1-primed T-lymphocytes and neural/glial antigens in OCHSC tissue could give rise to a stimulatory agent, which may in turn serve as the requisite signal 2 necessary to propel pro-inflammatory downstream cascades in signal-1-primed cells, i.e. LPS-PBMCs, and as a result PBMCs become immunoreactive.

I_A and I_D are voltage-gated delayed rectifying K^+ channels (K_v) that become active at voltages close to action potential threshold, and are known to dampen excitation and intrinsically shape action potential waveform (26). Although the identity of the molecular K_v subunits that comprise I_A and I_D is not fully defined, I_D is believed to be mediated by α-dendrotoxin sensitive K_v1 subunits, i.e. $K_v1.1$, $K_v1.2$ and $K_v1.6$, which in addition to being found at the soma and proximal dendrites, are strongly expressed in the axonal initial segment (51, 52). In contrast, I_A is a somatodendritic current whose density increases with distance from the soma (53) and is presumed to be primarily constituted by the K_v4 subunits $K_v4.1$, $K_v4.2$ and $K_v4.3$ (54). Our data suggests that the inflammasome-associated hyperexcitability exhibited by cortical and hippocampal neurons in OCHSCs is partially mediated by the 4-AP sensitive I_A and I_D hyperpolarizing currents. Several other studies have identified a similar correlation between CNS inflammatory insults and aberrant changes of 4-AP sensitive currents that underlie neuronal hyperexcitability. For example,

modeling systemic infections in rats by means of LPS intraperitoneal injections exacerbated 4-AP-induced epileptiform burst discharges in the hippocampus compared to saline (6). In addition, acute sterile insults known to trigger neuroinflammation in rodent models, such as ischemic and traumatic brain injury (55, 56), enhanced seizure susceptibility through reduction of I_A in CA1 pyramidal neurons up to one week following traumatic brain injury insult (57). A separate report found that ischemia-hypoxia increased the firing frequency of dorsal root ganglion neurons, which was provoked by I_D-mediated extension of APR (58). Further studies could establish whether inhibition of I_A and I_D in OCHSC neurons incubated with immunogen-stimulated PBMCs could lead to lowering network convulsive threshold in the presence of chemoconvulsants, like kainic acid, thus potentially facilitating epileptiform activity.

Although adding IR-PBMCs to OCHSCs in our in vitro model produced the same diminishing effect on I_A and I_D amplitude in cortical or hippocampal pyramidal neurons, prolongation of APR was only manifested by hippocampal neurons. This discrepancy in PBMC-induced elongation of action potential waveform between cortical and hippocampal neurons could be attributed to different I_A participation to the total hyperpolarizing current during the repolarization phase in cortical and the hippocampal pyramidal neurons. Indeed, while application of 4 mM of 4-AP to cortical layer II/III pyramidal neurons reportedly resulted in extending action potential duration by ~ 42% (59), CA1 and CA3 hippocampal pyramidal neurons exhibited far more drastic broadening of action potential waveform (CA3: ~310%; CA1: >200%) caused by adding 2-2.5 mM of 4-AP (26, 60), thus, suggesting that inflammation-induced decrease of I_A displayed by cortical neurons had marginal impact on the kinetics of membrane potential changes during cell firing compared to that in hippocampal neurons. Future experiments will reveal whether inflammasome activation could induce expression perturbance of the major subunits comprising I_A, i.e. K_v4, and I_D, i.e. K_v1. Also, because inflammasomes could reduce other types of outward currents activated during the repolarization phase, such as K^+ current of the delayed rectification (I_{KDR}) and K^+ currents activated by intracellular Ca^{2+} (I_{KCA}) (61), investigation of possible inflammation-induced changes of other components of the hyperpolarizing current during pyramidal cell firing is warranted.

Finally, Caspase-1 inhibition counteracted the culmination of neuroinflammation and hyperexcitability when immunogen-treated PBMCs were applied to OCHSCs in our co-culture model, indicating that peripheral inflammasome transduction into CNS cells requires Caspase-1-dependent pathways. Interestingly, deletion of genes encoding NLRP3 and ASC significantly inhibited T-lymphocyte extravasation in the experimental autoimmune encephalomyelitis mouse model of multiple sclerosis (21). Furthermore, in rheumatoid arthritis and dermatitis animal models, VX-765 attenuated peripheral inflammation by inhibiting PBMCs release of IL-1β and IL-18 (62). Thus, our results are consistent with findings by other groups suggesting that targeting interleukin conversion proved to be neuroprotective. In addition, several experimental models have shown that modulation of regulators of IL-1β biosynthesis, chiefly Caspase-1, was detrimental to seizure precipitation. In one study, knocking out Caspase-1 rendered mice significantly more resistant to seizures (36), while two separate studies reported that knockdown of RNA coding for NLRP1, NLRP3 and Caspase-1 reduced ictogenesis (38, 63). Also, targeting Caspase-1 cleavage, through systemic administration of VX-765 in mice, has been shown to have anticonvulsant

effects during pharmacologically induced seizures (37). Hence, our data is in agreement with other reports demonstrating that pharmacological modulation of inflammasomes is a candidate approach to alleviate hyperexcitability co-morbid with neuroinflammatory response. Notably, we also determined that blockade of Caspase-1 activation in our model prevented I_A- and I_D-mediated hyperexcitability in pyramidal neurons, suggesting that the Caspase-1-dependent interleukin conversion cascade acts -either directly or indirectly- as a neuromodulator, thereby modifying the activity of membrane ion channels.

Overall, the model presented herein provides novel insights into the mechanisms underlying predisposition of neuronal networks to hyperexcitation following an insult extrinsic to the CNS, specifically when inflammatory signals are transduced to the CNS through peripheral immune cells.

Conclusion

The main findings of our study are that while, ordinarily, infiltration of peripheral immune cells is innocuous, extravasation as a consequence of systemic inflammation can be pathogenic to the brain, resulting in aberrant excitability in pyramidal neurons. We found that in the cortex, the pathogenicity of peripheral inflammation in immunogenically-primed PBMCs was relatively limited, when compared to immunogenically-activated PBMCs, suggesting that the degree of immunogenicity of infiltrating cells predicates the extent of immune response in cortical cells. In contrast, we show that the hippocampus displayed the same vulnerability to both immunogenically-primed and immunogenically-activated PBMCs, with alteration of neuronal intrinsic properties being comparable between primed and activated PBMCs. Yet, in the case of primed PBMCs, transduction of pro-inflammatory signals seems to be dependent on cell-cell contact between PBMCs and the hippocampal tissue. Finally, by targeting inflammasome assembly, we found that inflammation-induced excitation in hippocampal neurons was mediated through Caspase-1 downstream effectors, where Caspase-1 activation results in enhancing neuronal excitability by diminishing 4-AP sensitive K^+ currents that dampen neuronal membrane excitability, namely I_D and I_A. Hence, we provide evidence that Caspase-1-activating inflammasome cascades can regulate functional properties of 4-AP sensitive K^+ channels in pyramidal neurons, which might help develop therapeutic approaches targeting Caspase-1 in order to control neuroinflammation and hyperexcitability following systemic infections or injuries.

Abbreviations

4-AP:4-aminopyridine; ACSF:Artificial cerebrospinal fluid; APR:Action potential repolarization; ASC:Associated speck-like protein containing a carboxy-terminal CARD; Ca^{2+}:Calcium; CFSE:Carboxyfluorescein diacetate succinimidyl ester; $CFSE^+$:CFSE-labeled; C_m:Cell membrane capacitance; CNS:Central nervous system; CTL:Control; DAPI:4',6-diamidino-2-phenylindole; DIV:Days in vitro; I_A:A-type fast activating, fast inactivating voltage-dependent K^+ current; I_D:D-type fast activating, slowly inactivating voltage-dependent K^+ current; I_{KCA}:K^+ currents activated by intracellular Ca^{2+}; I_{KDR}:K^+ current of the delayed rectification; IL:Interleukin; IR:Immunoreactive; I-V:Current-voltage; K^+:Potassium;

K_v:Voltage-gated potassium channels; LPS:Lipopolysaccharide; m:Media incubation of PBMCs; Mg^{2+}:Magnesium; Na^+:Sodium; NLR:NOD-like receptor; NLRP3:NLR Family Pyrin Domain Containing 3; OCHSCs:Organotypic cortico-hippocampal brain slice cultures; P:Postnatal day; PBMCs:Peripheral blood mononuclear cells; PBS:Phosphate buffered saline; Pro-:Precursor form; R_{in}:Input resistance; SEM:Standard error of mean; TLR:Toll-like receptor.

Declarations

Ethics approval and consent to participate

All procedures involving animals were performed in accordance with institutional policies and guidelines (Protocol #603, CIBPAR, Sainte-Justine Hospital Research Centre, Université de Montréal, Montreal, QC, Canada).

Consent for publication

Not applicable

Availability of supporting data and materials

All data generated or analyzed for this study is included in this published article. Any additional information will be made available by the corresponding author upon request.

Competing interests

The authors declare no competing interests.

Funding

This work was supported by Fondation Charles Guidon pour l'épilepsie (A.G.W.).

Authors' contributions

T.S. conceived, designed and performed most of the experiments. B.C. assisted with immunohistochemistry and performed all confocal imaging. Data was analyzed by T.S. and B.C. The manuscript was written by T.S., with assistance from B.C., and edited by all authors. A.G.W., B.A. and G.D.C. contributed to this work through supervision, equipment, reagents, technical and intellectual assistance. All authors read and approved the final version of the manuscript.

Acknowledgements

We thank Dr. Lionel Carmant at Université de Montréal for helping with experimental design, supervising part of the experiments conducted in this study, and providing funding through Canadian Institutes of Health Research. We thank Dr. William Colmers and Dr. Christopher Power at the University of Alberta

(Edmonton, Alberta) for providing insightful input and technical assistance on the conception and design of the project. We thank Dr. Nathalie Sanon and Mr. Abdulrahman Elhassan for technical assistance.

References

1. Kramer U, Chi CS, Lin KL, Specchio N, Sahin M, Olson H, et al. Febrile infection-related epilepsy syndrome (FIRES): pathogenesis, treatment, and outcome: a multicenter study on 77 children. Epilepsia. 2011;52(11):1956-65.
2. Dube CM, Brewster AL, Richichi C, Zha Q, Baram TZ. Fever, febrile seizures and epilepsy. Trends Neurosci. 2007;30(10):490-6.
3. Nabbout R. Autoimmune and inflammatory epilepsies. Epilepsia. 2012;53 Suppl 4:58-62.
4. Cusick MF, Libbey JE, Patel DC, Doty DJ, Fujinami RS. Infiltrating macrophages are key to the development of seizures following virus infection. J Virol. 2013;87(3):1849-60.
5. Libbey JE, Kennett NJ, Wilcox KS, White HS, Fujinami RS. Interleukin-6, produced by resident cells of the central nervous system and infiltrating cells, contributes to the development of seizures following viral infection. J Virol. 2011;85(14):6913-22.
6. Galic MA, Riazi K, Heida JG, Mouihate A, Fournier NM, Spencer SJ, et al. Postnatal inflammation increases seizure susceptibility in adult rats. J Neurosci. 2008;28(27):6904-13.
7. Galic MA, Riazi K, Pittman QJ. Cytokines and brain excitability. Front Neuroendocrinol. 2012;33(1):116-25.
8. Becker CE, O'Neill LA. Inflammasomes in inflammatory disorders: the role of TLRs and their interactions with NLRs. Semin Immunopathol. 2007;29(3):239-48.
9. Munoz-Planillo R, Kuffa P, Martinez-Colon G, Smith BL, Rajendiran TM, Nunez G. K(+) efflux is the common trigger of NLRP3 inflammasome activation by bacterial toxins and particulate matter. Immunity. 2013;38(6):1142-53.
10. Cruz CM, Rinna A, Forman HJ, Ventura AL, Persechini PM, Ojcius DM. ATP activates a reactive oxygen species-dependent oxidative stress response and secretion of proinflammatory cytokines in macrophages. J Biol Chem. 2007;282(5):2871-9.
11. Mariathasan S, Monack DM. Inflammasome adaptors and sensors: intracellular regulators of infection and inflammation. Nat Rev Immunol. 2007;7(1):31-40.
12. Bauernfeind FG, Horvath G, Stutz A, Alnemri ES, MacDonald K, Speert D, et al. Cutting edge: NF-kappaB activating pattern recognition and cytokine receptors license NLRP3 inflammasome activation by regulating NLRP3 expression. J Immunol. 2009;183(2):787-91.
13. Martinon F, Burns K, Tschopp J. The inflammasome: a molecular platform triggering activation of inflammatory caspases and processing of proIL-beta. Mol Cell. 2002;10(2):417-26.
14. Mariathasan S, Weiss DS, Newton K, McBride J, O'Rourke K, Roose-Girma M, et al. Cryopyrin activates the inflammasome in response to toxins and ATP. Nature. 2006;440(7081):228-32.

15. DeSena AD, Do T, Schulert GS. Systemic autoinflammation with intractable epilepsy managed with interleukin-1 blockade. J Neuroinflammation. 2018;15(1):38.
16. Liu Z, Xian H, Ye X, Chen J, Ma Y, Huang W. Increased levels of NLRP3 in children with febrile seizures. Brain Dev. 2020.
17. Dinarello CA. Overview of the IL-1 family in innate inflammation and acquired immunity. Immunol Rev. 2018;281(1):8-27.
18. Bernardino L, Balosso S, Ravizza T, Marchi N, Ku G, Randle JC, et al. Inflammatory events in hippocampal slice cultures prime neuronal susceptibility to excitotoxic injury: a crucial role of P2X7 receptor-mediated IL-1beta release. J Neurochem. 2008;106(1):271-80.
19. Hailer NP, Jarhult JD, Nitsch R. Resting microglial cells in vitro: analysis of morphology and adhesion molecule expression in organotypic hippocampal slice cultures. Glia. 1996;18(4):319-31.
20. Kebir H, Carmant L, Fontaine F, Beland K, Bosoi CM, Sanon NT, et al. Humanized mouse model of Rasmussen's encephalitis supports the immune-mediated hypothesis. J Clin Invest. 2018;128(5):2000-9.
21. Inoue M, Williams KL, Gunn MD, Shinohara ML. NLRP3 inflammasome induces chemotactic immune cell migration to the CNS in experimental autoimmune encephalomyelitis. Proc Natl Acad Sci U S A. 2012;109(26):10480-5.
22. Fernandes-Alnemri T, Wu J, Yu JW, Datta P, Miller B, Jankowski W, et al. The pyroptosome: a supramolecular assembly of ASC dimers mediating inflammatory cell death via caspase-1 activation. Cell Death Differ. 2007;14(9):1590-604.
23. Faustin B, Lartigue L, Bruey JM, Luciano F, Sergienko E, Bailly-Maitre B, et al. Reconstituted NALP1 inflammasome reveals two-step mechanism of caspase-1 activation. Mol Cell. 2007;25(5):713-24.
24. Ficker E, Heinemann U. Slow and fast transient potassium currents in cultured rat hippocampal cells. J Physiol. 1992;445:431-55.
25. Thompson SH. Three pharmacologically distinct potassium channels in molluscan neurones. J Physiol. 1977;265(2):465-88.
26. Mitterdorfer J, Bean BP. Potassium currents during the action potential of hippocampal CA3 neurons. J Neurosci. 2002;22(23):10106-15.
27. Zou Z, Lu Y, Zha Y, Yang H. Endocannabinoid 2-Arachidonoylglycerol Suppresses LPS-Induced Inhibition of A-Type Potassium Channel Currents in Caudate Nucleus Neurons Through CB1 Receptor. J Mol Neurosci. 2016;59(4):493-503.
28. Storm JF. Temporal integration by a slowly inactivating K+ current in hippocampal neurons. Nature. 1988;336(6197):379-81.
29. Storm JF. Action potential repolarization and a fast after-hyperpolarization in rat hippocampal pyramidal cells. J Physiol. 1987;385:733-59.
30. Flores J, Noel A, Foveau B, Lynham J, Lecrux C, LeBlanc AC. Caspase-1 inhibition alleviates cognitive impairment and neuropathology in an Alzheimer's disease mouse model. Nat Commun.

2018;9(1):3916.

31. Zhang Y, Liu L, Liu YZ, Shen XL, Wu TY, Zhang T, et al. NLRP3 Inflammasome Mediates Chronic Mild Stress-Induced Depression in Mice via Neuroinflammation. Int J Neuropsychopharmacol. 2015;18(8).
32. Heneka MT, Kummer MP, Latz E. Innate immune activation in neurodegenerative disease. Nat Rev Immunol. 2014;14(7):463-77.
33. Riazi K, Galic MA, Pittman QJ. Contributions of peripheral inflammation to seizure susceptibility: cytokines and brain excitability. Epilepsy Res. 2010;89(1):34-42.
34. Freeman LC, Ting JP. The pathogenic role of the inflammasome in neurodegenerative diseases. J Neurochem. 2016;136 Suppl 1:29-38.
35. Mamik MK, Power C. Inflammasomes in neurological diseases: emerging pathogenic and therapeutic concepts. Brain. 2017;140(9):2273-85.
36. Ravizza T, Lucas SM, Balosso S, Bernardino L, Ku G, Noe F, et al. Inactivation of caspase-1 in rodent brain: a novel anticonvulsive strategy. Epilepsia. 2006;47(7):1160-8.
37. Maroso M, Balosso S, Ravizza T, Iori V, Wright CI, French J, et al. Interleukin-1beta biosynthesis inhibition reduces acute seizures and drug resistant chronic epileptic activity in mice. Neurotherapeutics. 2011;8(2):304-15.
38. Tan CC, Zhang JG, Tan MS, Chen H, Meng DW, Jiang T, et al. NLRP1 inflammasome is activated in patients with medial temporal lobe epilepsy and contributes to neuronal pyroptosis in amygdala kindling-induced rat model. J Neuroinflammation. 2015;12:18.
39. Semmler A, Okulla T, Sastre M, Dumitrescu-Ozimek L, Heneka MT. Systemic inflammation induces apoptosis with variable vulnerability of different brain regions. J Chem Neuroanat. 2005;30(2-3):144-57.
40. Ban E, Milon G, Prudhomme N, Fillion G, Haour F. Receptors for interleukin-1 (alpha and beta) in mouse brain: mapping and neuronal localization in hippocampus. Neuroscience. 1991;43(1):21-30.
41. Takao T, Tracey DE, Mitchell WM, De Souza EB. Interleukin-1 receptors in mouse brain: characterization and neuronal localization. Endocrinology. 1990;127(6):3070-8.
42. Ban EM. Interleukin-1 receptors in the brain: characterization by quantitative in situ autoradiography. Immunomethods. 1994;5(1):31-40.
43. Shrestha R, Millington O, Brewer J, Dev KK, Bushell TJ. Lymphocyte-mediated neuroprotection in in vitro models of excitotoxicity involves astrocytic activation and the inhibition of MAP kinase signalling pathways. Neuropharmacology. 2014;76 Pt A:184-93.
44. Kigerl KA, Ankeny DP, Garg SK, Wei P, Guan Z, Lai W, et al. System x(c)(-) regulates microglia and macrophage glutamate excitotoxicity in vivo. Exp Neurol. 2012;233(1):333-41.
45. Yawata I, Takeuchi H, Doi Y, Liang J, Mizuno T, Suzumura A. Macrophage-induced neurotoxicity is mediated by glutamate and attenuated by glutaminase inhibitors and gap junction inhibitors. Life Sci. 2008;82(21-22):1111-6.

46. Marchi N, Johnson AJ, Puvenna V, Johnson HL, Tierney W, Ghosh C, et al. Modulation of peripheral cytotoxic cells and ictogenesis in a model of seizures. Epilepsia. 2011;52(9):1627-34.
47. Deprez F, Zattoni M, Mura ML, Frei K, Fritschy JM. Adoptive transfer of T lymphocytes in immunodeficient mice influences epileptogenesis and neurodegeneration in a model of temporal lobe epilepsy. Neurobiol Dis. 2011;44(2):174-84.
48. Xu D, Robinson AP, Ishii T, Duncan DS, Alden TD, Goings GE, et al. Peripherally derived T regulatory and gammadelta T cells have opposing roles in the pathogenesis of intractable pediatric epilepsy. J Exp Med. 2018;215(4):1169-86.
49. Carson MJ, Reilly CR, Sutcliffe JG, Lo D. Mature microglia resemble immature antigen-presenting cells. Glia. 1998;22(1):72-85.
50. Dulken BW, Buckley MT, Navarro Negredo P, Saligrama N, Cayrol R, Leeman DS, et al. Single-cell analysis reveals T cell infiltration in old neurogenic niches. Nature. 2019;571(7764):205-10.
51. Monaghan MM, Trimmer JS, Rhodes KJ. Experimental localization of Kv1 family voltage-gated K+ channel alpha and beta subunits in rat hippocampal formation. J Neurosci. 2001;21(16):5973-83.
52. Kole MH, Letzkus JJ, Stuart GJ. Axon initial segment Kv1 channels control axonal action potential waveform and synaptic efficacy. Neuron. 2007;55(4):633-47.
53. Hoffman DA, Magee JC, Colbert CM, Johnston D. K+ channel regulation of signal propagation in dendrites of hippocampal pyramidal neurons. Nature. 1997;387(6636):869-75.
54. Serodio P, Rudy B. Differential expression of Kv4 K+ channel subunits mediating subthreshold transient K+ (A-type) currents in rat brain. J Neurophysiol. 1998;79(2):1081-91.
55. de Rivero Vaccari JP, Lotocki G, Alonso OF, Bramlett HM, Dietrich WD, Keane RW. Therapeutic neutralization of the NLRP1 inflammasome reduces the innate immune response and improves histopathology after traumatic brain injury. J Cereb Blood Flow Metab. 2009;29(7):1251-61.
56. Abulafia DP, de Rivero Vaccari JP, Lozano JD, Lotocki G, Keane RW, Dietrich WD. Inhibition of the inflammasome complex reduces the inflammatory response after thromboembolic stroke in mice. J Cereb Blood Flow Metab. 2009;29(3):534-44.
57. Lei Z, Deng P, Li J, Xu ZC. Alterations of A-type potassium channels in hippocampal neurons after traumatic brain injury. J Neurotrauma. 2012;29(2):235-45.
58. Gruss M, Ettorre G, Stehr AJ, Henrich M, Hempelmann G, Scholz A. Moderate hypoxia influences excitability and blocks dendrotoxin sensitive K+ currents in rat primary sensory neurones. Mol Pain. 2006;2:12.
59. Pathak D, Guan D, Foehring RC. Roles of specific Kv channel types in repolarization of the action potential in genetically identified subclasses of pyramidal neurons in mouse neocortex. J Neurophysiol. 2016;115(5):2317-29.
60. Spigelman I, Zhang L, Carlen PL. Patch-clamp study of postnatal development of CA1 neurons in rat hippocampal slices: membrane excitability and K+ currents. J Neurophysiol. 1992;68(1):55-69.

61. Brown DA, Gahwiler BH, Griffith WH, Halliwell JV. Membrane currents in hippocampal neurons. Prog Brain Res. 1990;83:141-60.
62. Wannamaker W, Davies R, Namchuk M, Pollard J, Ford P, Ku G, et al. (S)-1-((S)-2-{[1-(4-amino-3-chloro-phenyl)-methanoyl]-amino}-3,3-dimethyl-butanoy l)-pyrrolidine-2-carboxylic acid ((2R,3S)-2-ethoxy-5-oxo-tetrahydro-furan-3-yl)-amide (VX-765), an orally available selective interleukin (IL)-converting enzyme/caspase-1 inhibitor, exhibits potent anti-inflammatory activities by inhibiting the release of IL-1beta and IL-18. J Pharmacol Exp Ther. 2007;321(2):509-16.
63. Meng XF, Tan L, Tan MS, Jiang T, Tan CC, Li MM, et al. Inhibition of the NLRP3 inflammasome provides neuroprotection in rats following amygdala kindling-induced status epilepticus. J Neuroinflammation. 2014;11:212.

Figures

FIG. 1

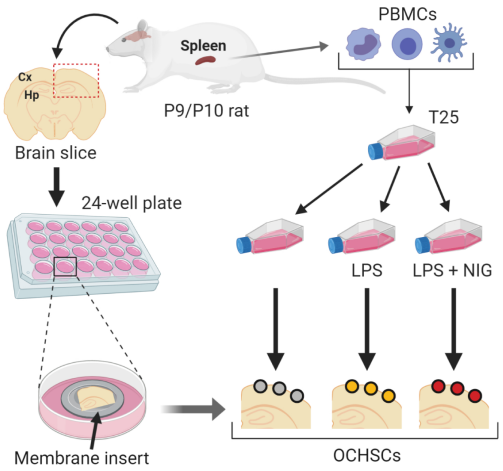

Figure 1

Establishment of the PBMC-OCHSC co-culture system. Schematic illustration showing the experimental design of the in vitro model. Brain slices were prepared from of P9/P10 Sprague-Dawley male rats, where slices were trimmed to only contain the cortex (Cx) and the hippocampus (Hp) from each hemisphere. To obtain OCHSCs, slices were individually placed on top a membrane inset and grown in 24-well plates supplied with culture media. PBMCs were simultaneously extracted from the spleen of the same rat and

cultured in T25 flasks. At 3 DIV, PBMCs were divided into three different flasks. At 6 DIV, the first flask was treated with LPS for 3-3.5 hours followed by nigericin (NIG) for 2.5-3 hours (red circles), the second was only treated with LPS for 3-3.5 hours (yellow circles), and the third was left untreated (grey circles). After washing out the drugs, PBMCs from each flask were concentrated, and ~3.0 × 104 cells were added on top of the cortex of each OCHSC.

FIG. 2

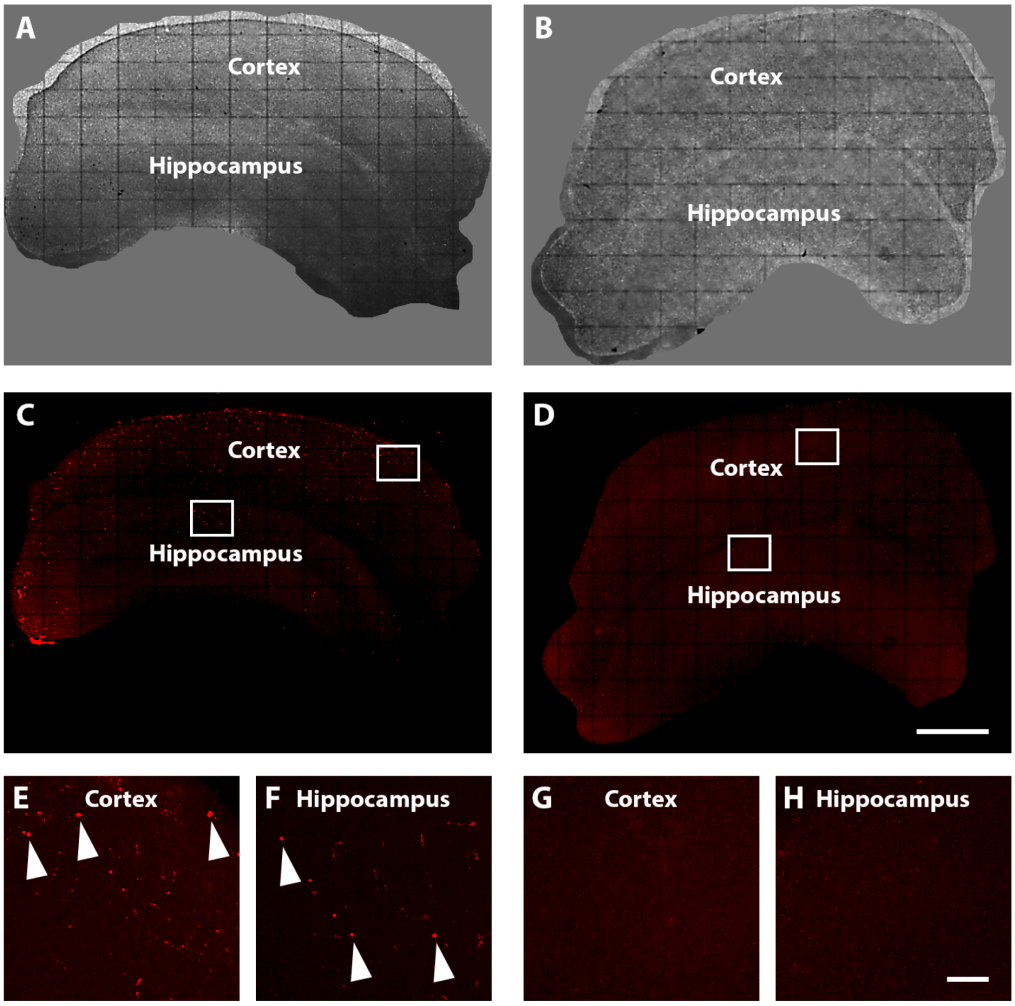

Figure 2

The OCHSC membrane insert acts as a barrier by preventing PBMCs infiltration. (A-D) Mosaic images stitched to show OCHSCs co-cultured with CFSE+ PBMCs added on top of the cortex (A, C), and OCSHCs co-cultured with CFSE+ PBMCs added to the media where OCHSCs and PBMCs are separated by the membrane insert (B, D), viewed in bright field (A, B) and under fluorescent light (C, D). (E-H) Insets of white boxes in C and D, showing the cortex (E, G) and the hippocampus (F, H) of OCHSCs co-cultured directly with CFSE+ PBMCs (E, F) and OCHSCs co-cultured separately from media-incubated CFSE+ PBMCs (G, H). White arrowheads in E and F mark CFSE+ PBMCs respectively adhering to cortical and hippocampal tissue in OCHSCs. Scale bars, 1 mm (A-D), 100 μm (E-H).

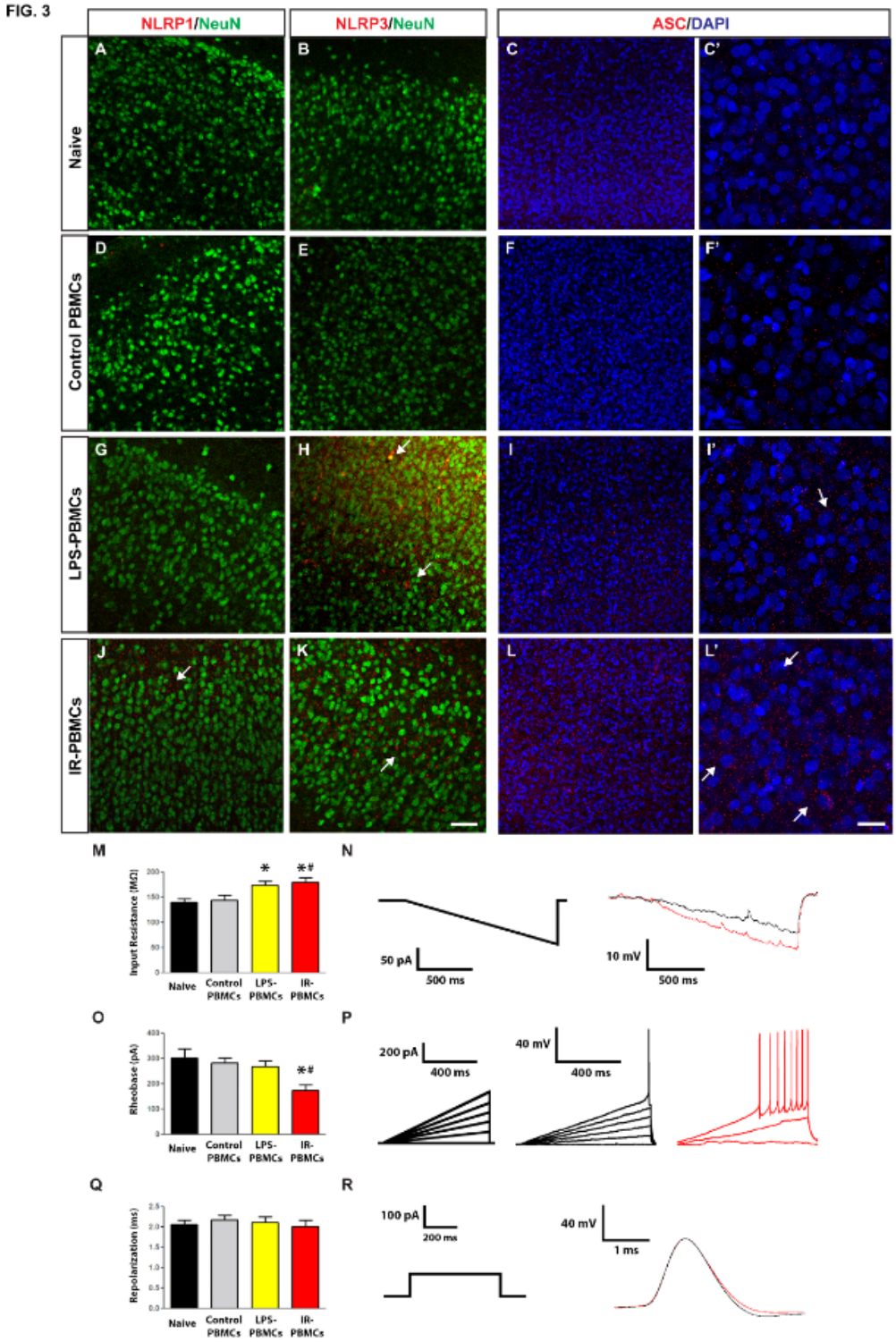

Figure 3

Pro-inflammatory PBMCs induce neuroinflammation and hyperexcitability in the cortex. (A-L´) Representative images of cortical tissue showing immunohistochemical double-staining of NLRP1/NeuN (A, D, G, J), NLRP3/NeuN (B, E, H, K) and ASC/DAPI (C, C´, F, F´, I, I´, L, L´) in naive OCHSCs (A-C´) as compared to OCHSCs co-cultured with control PBMCs (D-F´), LPS-PBMCs (G-I´) and IR-PBMCs (J-L´). C´, F´, I´, L´ are magnified images of white boxes in C, F, I, L, respectively. White arrows denote ectopic

expression of NLRP1 in J, NLRP3 in H and K, and ASC in I´ and L´. (M, O, Q) Bar graphs comparing the electrophysiological properties of pyramidal neurons in the cortex of naive OCHSCs to those of OCHSCs co-cultured with control PBMCs, LPS-PBMCs and IR-PBMCs with respect to input resistance (M), rheobase (O), and repolarization time (Q). (N, P, R) Representative input current traces and voltage response traces of: (N) a hyperpolarizing 100 pA ramp (left) and cell response (right), (P) depolarizing 100 pA ramps in 100 pA increments (left) and cell response (middle, right), and (R) a depolarizing 100 pA step current injection (left) and cell response (right), of cortical pyramidal neurons from naive OCHSCs (black) and OCHSCs co-cultured with IR-PBMCs (red) recorded in in current-clamp. Error bars represent mean ± SEM; *$p < 0.05$ compared to naive, #$p < 0.05$ compared to control PBMCs by Bonferroni test. Scale bars, 100 μm (A-L), 50 μm (C´-L´).

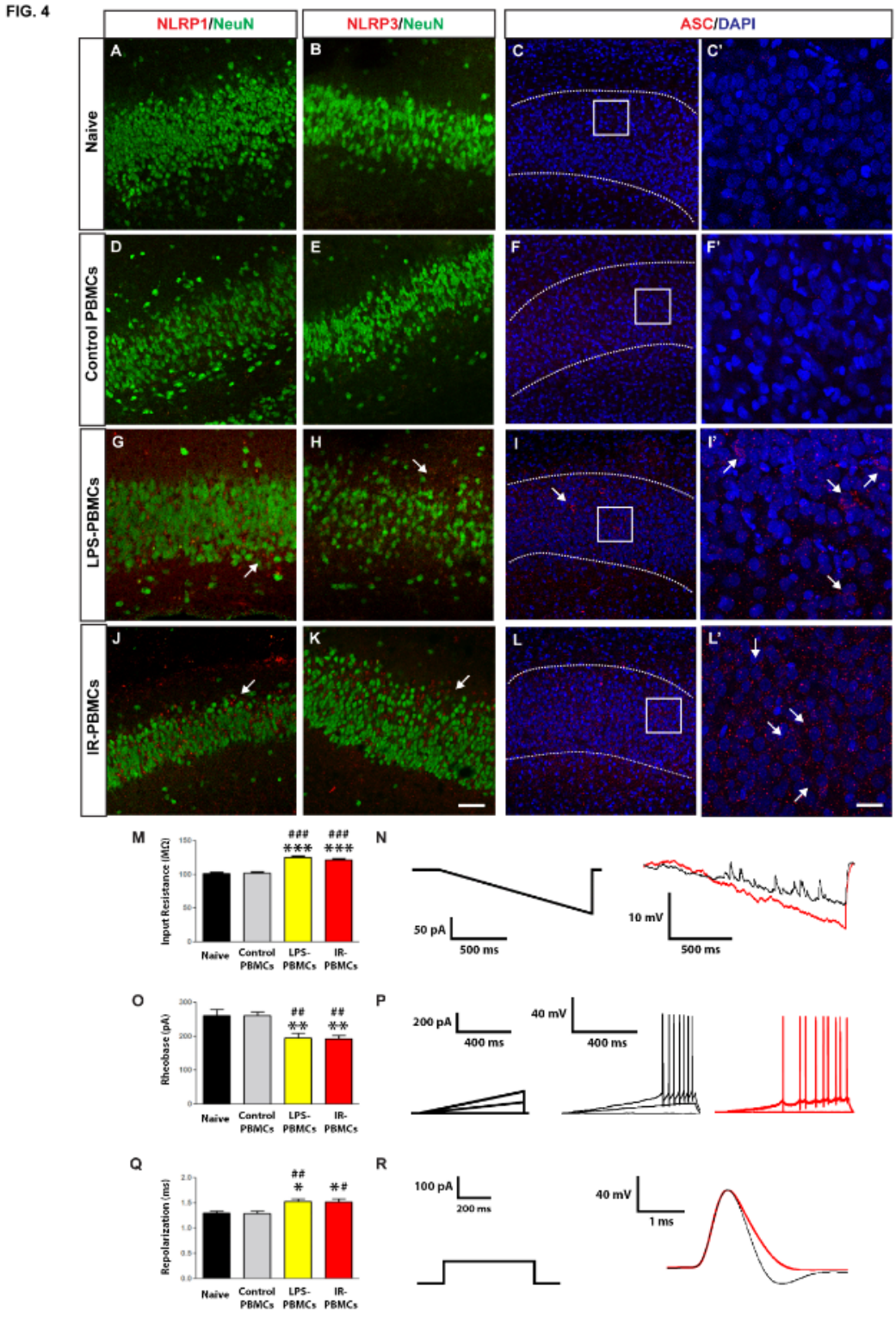

Figure 4

Priming inflammation in PBMCs is sufficient to induce neuroinflammation and hyperexcitability in the hippocampus. (A-L´) Representative images of immunohistochemical double-staining of NLRP1/NeuN (A, D, G, J), NLRP3/NeuN (B, E, H, K) and ASC/DAPI (C, C´, F, F´, I, I´, L, L´) in hippocampal tissue of naive OCHSCs (A-C´) in comparison with OCHSCs co-cultured with control PBMCs (D-F´), LPS-PBMCs (G-I´) and IR-PBMCs (J-L´). C´, F´, I´, L´ are magnified images of white boxes in C, F, I, L, respectively. White arrows

denote ectopic expression of NLRP1 in J, NLRP3 in H, K, and ASC in I´, L´. (M, O, Q) Bar graphs comparing pyramidal neurons in the hippocampus of naive OCHSCs to those of OCHSCs co-cultured with control PBMCs, LPS-PBMCs and IR-PBMCs with respect to input resistance (M), rheobase (O), and repolarization time (Q). (N, P, R) Representative input current traces and voltage response traces of: (N) a hyperpolarizing 100 pA ramp (left) and cell response (right), (P) depolarizing 100 pA ramps in 100 pA increments (left) and cell response (middle, right), and (R) a depolarizing 100 pA step current injection (left) and cell response (right), of hippocampal pyramidal neurons from naive OCHSCs (black) and OCHSCs co-cultured with IR-PBMCs (red) recorded in in current-clamp. Error bars represent mean ± SEM; *p < 0.05, **p < 0.01, ***p < 0.001 compared to naive, #p < 0.05, ##p < 0.01, ###p < 0.001 compared to control PBMCs by Bonferroni test. Scale bars, 100 µm (A-L), 50 µm (C´-L´).

FIG. 5

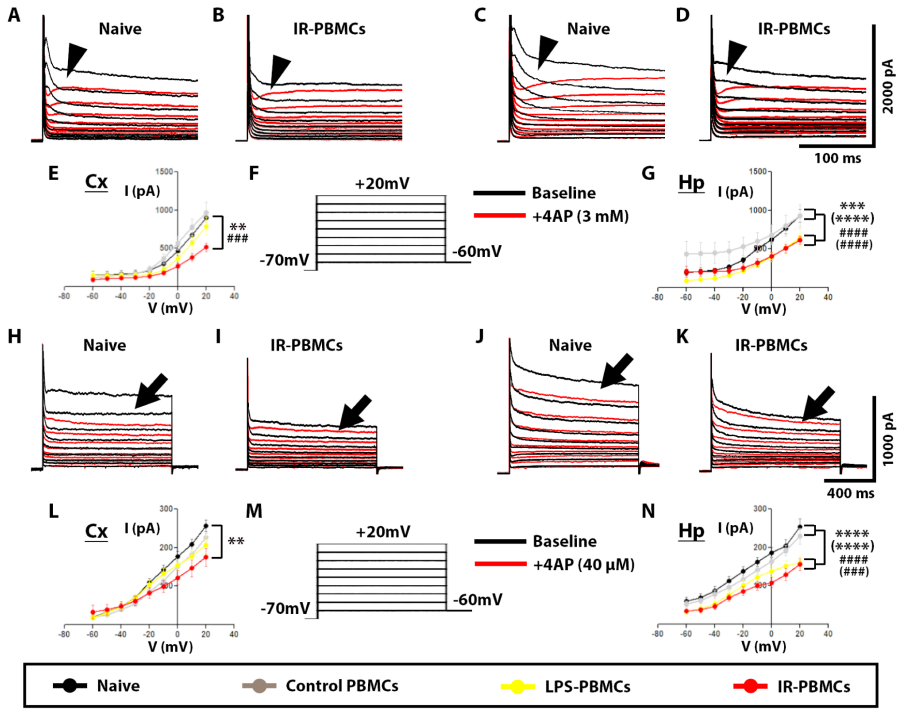

Figure 5

Transduction of peripheral inflammation impairs 4-AP sensitive currents in cortical and hippocampal neurons. (A-D, H-K) Representative current outputs of IA (A-D) and ID (H-K) traces of cortical (A, B, H, I) and hippocampal (C, D, J, K) pyramidal neurons in naive OCHSCs (A, C, H, J) and OCHSCs co-cultured with IR-PBMCs (B, D, I, K) obtained in response to +10 mV incremental depolarizing voltage steps between −60 and +20 mV while constantly holding the cells at -70 mV in voltage-clamp (F, M). Cells were first recorded

in baseline conditions (baseline; black traces), and subsequently recorded following the perfusion of 3 mM (A-D) or 40 μM (H-K) 4-AP to respectively block IA and ID (+4-AP; red traces). (E, G, L, N) I-V graphs comparing IA (E, G) and ID (L, N), calculated by subtracting cell response after blocking 4-AP sensitive currents from baseline conditions, in naive OCHSCs (back) compared to OCHSCs co-cultured with control PBMCs (grey), LPS-PBMCs (yellow) and IR-PBMCs (red) in cortical (Cx) (E, L) and hippocampal (Hp) (G, N) pyramidal neurons. Black arrowheads in A, B, C, D denote the difference between baseline and 3 mM 4-AP traces, i.e. IA, at maximum input voltage (+20 mV); black arrows in H, I, J, K denote the difference between baseline and 40 μM 4-AP traces, i.e. ID, at +20 mV. Error bars represent mean ± SEM; **p < 0.01, ***p < 0.001, ****p < 0.0001 IR-PBMCs compared to naive, ###p < 0.001, ####p < 0.0001 IR-PBMCs compared to control PBMCs, (****)p < 0.0001 LPS-PBMCs compared to naive, (###)p < 0.001, (####)p < 0.0001 LPS-PBMCs compared to control PBMCs by Bonferroni test.

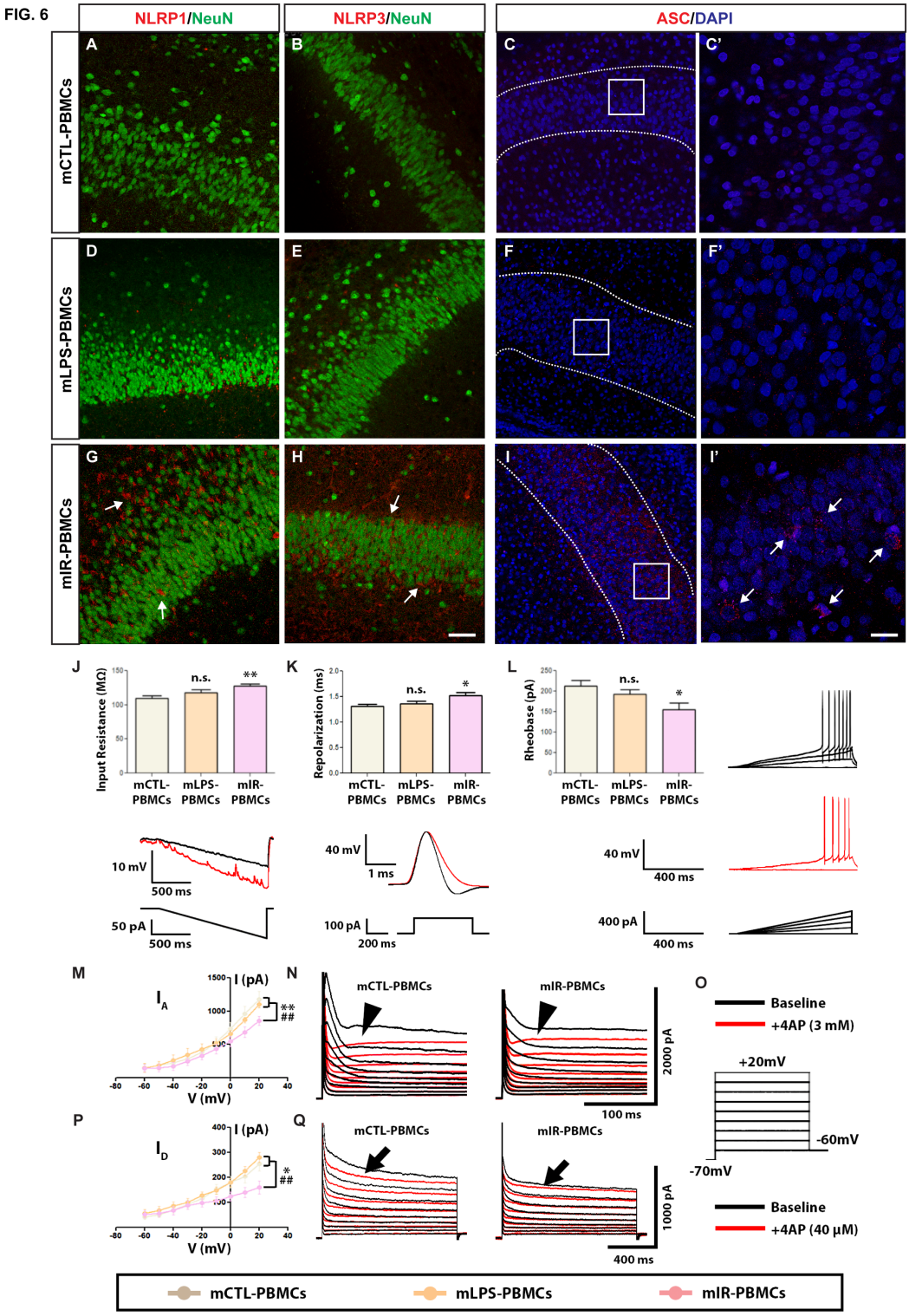

Figure 6

Cell-cell contact between LPS-PBMCs and OCHSCs is necessary for transduction of peripheral inflammation. (A-I´) Representative immunohistochemistry images of NLRP1/NeuN (A, D, G), NLRP3/NeuN (B, E, H) and ASC/DAPI (C, C´, F, F´, I, I´) in the hippocampus of OCHSCs incubated with mCTL-PBMCs (A-C´), mLPS-PBMCs (D-F´) and mIR-PBMCs (G-I´). C´, F´, I´ are magnified images of white boxes in C, F, I, respectively. White arrows mark upregulation of NLRP1, NLRP3, and ASC in G, H, I´,

respectively. (J, K, L) (Top, J, K; top-left, L) Bar graphs comparing input resistance (J), repolarization time (K) and rheobase (L) of hippocampal pyramidal neurons in all experimental groups, (middle, J, K; top-right and middle-right, L) exemplary voltage output traces of input resistance (J), repolarization (K) and rheobase (L) in OCHSCs incubated with mCTL-PBMCs (black) and mIR-PBMCs (red), in response to input current traces for resistance (J, bottom), repolarization (K, bottom) and rheobase (L, bottom-right). Input protocols in J, K, L were the same as in Figures 4N, 4P, 4R, respectively. (M, P) I-V graphs comparing IA (M) and ID (P) of hippocampal neurons from OCHSCs incubated with mCTL-PBMCs (grey), LPS-PBMCs (orange) and IR-PBMCs (pink). (N, Q) Exemplary IA (N) and ID (Q) output traces in OCHSCs incubated with mCTL-PBMCs (left) and mIR-PBMCs (right) recorded in baseline conditions (baseline; black traces), and after applying 3 mM (N) and 40 µM (Q) 4-AP to respectively block IA and ID (+4-AP; red traces). (O) Voltage input trace (same as in Figure 5). Black arrowheads in N denote IA; black arrows in Q denote ID. Error bars represent mean ± SEM; n.s. denotes not significant, *p < 0.05, **p < 0.01, ****p < 0.0001 compared to mCTL-PBMCs; ##p < 0.01 compared to mLPS-PBMCs; p-values were calculated by Bonferroni test. Scale bars, 100 µm (A-I), 50 µm (C´-I´).

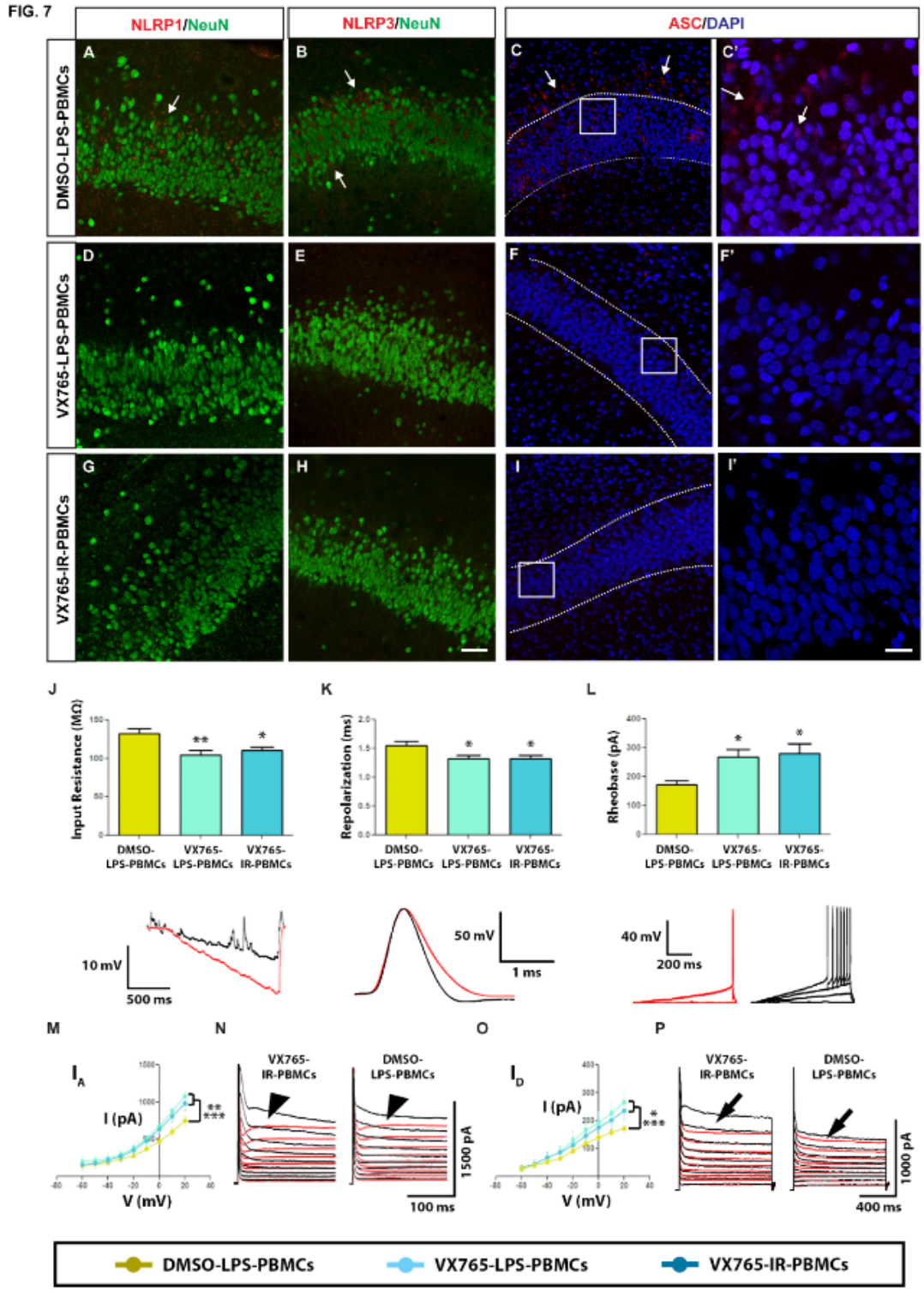

Figure 7

Inhibition of inflammasome assembly protected the hippocampus from inflammation transduction and inflammatory-coupled hyperexcitability. (A-I´) Representative images of double immunostaining of NLRP1/NeuN (A, D, G), NLRP3/NeuN (B, E, H) and ASC/DAPI (C, C´, F, F´, I, I´) in the hippocampus of OCHSCs co-cultured with DMSO-LPS-PBMCs (A-C´), VX765-LPS-PBMCs (D-F´) and VX765-IR-PBMCs (G-I´). C´, F´, I´ are magnified images of white boxes in C, F, I, respectively. White arrows mark upregulation of

NLRP1, NLRP3 and ASC in A, B, and C´, respectively. (J, K, L) (top) Bar graphs comparing input resistance (J), repolarization time (K) and rheobase (L) in OCHSC hippocampal neurons in all experimental groups, (bottom) exemplary current output traces in response to the voltage input protocols used in Figures 4N, 4P and 4R to respectively calculate input resistance (J), repolarization time (K) and rheobase (L) in OCHSCs cultured with VX765-IR-PBMCs (black) and DMSO-LPS-PBMCs (red). (M, O) I-V graphs comparing IA (M) and ID (O) of hippocampal neurons from OCHSCs co-cultured with DMSO-LPS-PBMCs (olive), VX765-LPS-PBMCs (light blue) and VX765-IR-PBMCs (navy blue). (N, P) Exemplary outputs of IA (N) and ID (P) traces in OCHSCs cultured with VX765-IR-PBMCs (left) and DMSO-LPS-PBMCs (right) recorded in baseline conditions (baseline; black traces), and following the application of 3mM (N) and 40 μM (P) 4-AP to baseline conditions to respectively block IA and ID (+4-AP; red traces) in response to the same input protocol used in Figure 5. Black arrowheads in N denote IA; black arrows in P denote ID. Error bars represent mean ± SEM; *p < 0.05, **p < 0.01, ***p < 0.001 compared to DMSO-LPS-PBMCs calculated by Bonferroni test. Scale bars, 100 μm (A-I), 50 μm (C´-I´).